Fall 12-10-2021

HYDROGEN PEROXIDE VAPOR DECONTAMINATION OF POLYLACTIC ACID FIBERS

Alexandra Craig
University of Texas at Tyler

HYDROGEN PEROXIDE VAPOR DECONTAMINATION OF POLYLACTIC ACID FIBERS

Alexandra Craig

A thesis submitted in partial fulfillment

of the requirements for the degree of

Master of Science

Department of Mechanical Engineering

Shih-Feng Chou, Ph.D., Committee Chair

College of Engineering

The University of Texas at Tyler
Tyler, Texas

This is to certify that the Master's Thesis of

ALEXANDRA CRAIG

has been approved for the thesis requirement on
November 5th, 2021
for the Master of Science in Mechanical Engineering degree

Approvals:

DocuSigned by:
Shih-Feng Chou
B32559E29B3244B...

Thesis Chair: Shih-Feng Chou, Ph.D.

DocuSigned by:
Fredericka Brown
74EBC2DA0375475...

Member: Fredericka Brown, Ph.D.

DocuSigned by:
Nelson Fumo
9BAB5E76B5E14AE...

Member: Nelson Fumo, Ph.D.

DocuSigned by:
Tahsin Khajah
ACA7690059AD419...

ME Graduate Coordinator, on behalf of
Chair, Department of Mechanical Engineering

DocuSigned by:
1AF8A43D33294C4...

Associate Dean, on behalf of
Dean, College of Engineering

The style and format of this thesis are in accordance with **Materials Science and Engineering C: Materials for Biological Applications**. The following referred journal papers and conference proceedings were products of the M.S. degree:

Referred Journal Articles:

[1] **A. Craig**, S.F. Chou, Effects of solvent mixing time and drug loading on the physico-mechanical properties and in vitro drug release behaviors of electrospun polylactic acid (PLA) fibers, J Mech. Behav. Biomed. Mater. (2021) in preparation for submission.

[2] **A. Craig**, S.F. Chou, Tensile properties and in vitro drug release behaviors of electrospun polylactic acid (PLA) fibers after various vapor phase hydrogen peroxide treatments, Polymers (2021) in preparation for submission.

[3] M. Small, A. Faglie, **A. Craig**, M. Pieper, V. Fernand Narcisse, P. Neuenschwander, S.F. Chou, Nanostructure-enabled and macromolecule-grafted surfaces for biomedical applications, Micromachines 9 (2018) 243. doi:10.3390/mi9050243.

Conference Proceedings:

[1] **A. Craig**, S.F. Chou, Electrospun drug-loaded polylactic acid fibers for wound dressings, in Proceedings of the 2021 Lyceum Research Showcase, (2021), Tyler TX. *2nd Place Graduate Posters.*

[2] **A. Craig**, S.F. Chou, Handheld vapor phase hydrogen peroxide decontamination device, in Proceedings of the 2020 Lyceum Research Showcase, (2020), Tyler TX.

[3] **A. Craig**, S.F. Chou, Handheld vapor phase hydrogen peroxide decontamination device, in Proceedings of the 2020 Great Plains Honors Council Conference, (2020), Virtual. *1st Place Britt Poster Awards: Over 60 Credits Hours- STEM.*

[4] **A. Craig**, S.F. Chou, Handheld vapor phase hydrogen peroxide decontamination device, in Proceedings of the 2019 National Collegiate Honors Council Conference, (2019), New Orleans LA. *1st Place Student Posters: SPUR Awards-Business, Engineering & Computer Science.*

[5] **A. Craig**, A.R. Faglie, S.F. Chou, Engineering approach to vapor phase hydrogen peroxide decontamination, in Proceedings of the 2019 ASEE Gulf-Southwest Section Annual Meeting, (2019), Tyler TX.

ACKNOWLEDGEMENT

I would like to first express my sincere gratitude to Dr. Shih-Feng Chou for giving me the opportunity to perform this research under his guidance and for his continuous support, patience, and encouragement. It has truly been a privilege to work with him on this research. I would like to give special thanks to my committee members, Dr. Fredericka Brown and Dr. Nelson Fumo, for their valuable advice and support. I would like to thank Addison Faglie and Aaron Wilson for their assistance and support, as well as other members of the Chou Biomaterials Lab for their support and encouragement. Lastly, I would like to thank my family and friends for their support and encouragement.

Abstract

HYDROGEN PEROXIDE VAPOR DECONTAMINATION OF POLYLACTIC ACID FIBERS

Alexandra Craig

Thesis Chair: Shih-Feng Chou, Ph.D.

The University of Texas at Tyler

November 2021

Electrospun fibers have attracted attentions in topical drug delivery due to the ability to modulate drug release at high drug loading. While the pharmaceutical properties of these drug-eluting fibers were reported elsewhere, the compatibility of these fibers with hydrogen peroxide vapor, an effective decontaminant, is not fully established. In this work, polylactic acid (PLA) microfibers loaded with acetylsalicylic acid (ASA) were electrospun to examine their compatibility with hydrogen peroxide vapor. Results suggested a strengthening effect of the PLA/ASA fibers due to intermolecular interactions of ASA with PLA, which modulated the in vitro drug release rates. After exposing PLA/ASA fibers to vapor phase hydrogen peroxide, results showed the disruptions of the intermolecular bonds between the ASA and PLA that reduced the mechanical properties and facilitated the burst release behaviors of the fibers. This work provided the scientific understanding on the role of drug-polymer interactions in electrospun fibers and their corresponding effects after exposure to hydrogen peroxide vapor.

Keywords: vapor phase hydrogen peroxide, decontamination, electrospun fibers, polylactic acid, drug-polymer interactions

TABLE OF CONTENTS

Chapter Page

1 INTRODUCTION 1

1.1 Topical Drug Delivery 1
1.2 Decontamination of the Drug delivery Systems 2
1.3 Thesis Hypothesis 4

2 SIGNIFICANCE 7

3 LITERATURE REVIEW 8

3.1 Drug Delivery Systems 8
3.1.1 Nanoparticles 8
3.1.2 Liposomes 9
3.1.3 Hydrogels 10
3.1.4 Scaffolds 10
3.1.5 Nanofibers 11
3.2 Electrospinning 12
3.3 Polylactic Acid (PLA) 14
3.3.1.1 Temperature 14
3.3.1.2 Oxidation 15
3.3.1.3 Hydrolytic 15
3.4 Decontamination Products 16
3.4.1 Contact Disinfectants 16
3.4.1.1 Sodium Hypochlorite 16
3.4.1.2 Alcohol 17
3.4.1.3 Glutaraldehyde 17
3.4.2 Non-contact Disinfectants 18
3.4.2.1 Ozone 18
3.4.2.2 Chlorine-releasing Agents 19
3.4.2.3 UV Light 19
3.5 Hydrogen Peroxide 20
3.5.1 Process 20
3.5.2 Safety 21
3.5.3 Potential Dangers 21
3.5.4 Material Compatibility 23
3.5.4.1 Metal 23
3.5.4.2 Polymers 24
3.5.4.3 Composite Materials 25
3.5.5 Efficacy 26

4 MATERIALS AND METHODS 28

4.1 Materials 28

4.2 Preparation of polymer solutions 28
4.3 Electrospinning of PLA/ASA fibers 29
4.4 Characterizations of electrospun fibers 29
4.4.1 Fiber morphologies 30
4.4.2 Fiber diameters 30
4.4.3 Fiber mat densities 30
4.4.4 Mechanical testing 30
4.4.5 In vitro drug release studies 31
4.5 Handheld hydrogen peroxide device 32
4.6 Hydrogen peroxide vapor calibration 33
4.7 Hydrogen peroxide vapor exposures on PLA fibers 35
4.8 PLA/ASA fibers after hydrogen peroxide vapor exposures 35
4.8.1 Fiber Morphology 36
4.8.2 Fiber Diameter 36
4.8.3 Weight Change 36
4.8.4 Area Change 36
4.8.5 Mechanical Testing 37
4.8.6 Fourier-Transform Infrared Spectroscopy (FTIR) 37
4.8.7 In vitro Drug Release Assay 37

5 RESULTS AND DISCUSSION 38

5.1 Electrospun drug-eluting polylactic acid fibers 38
5.1.1 Solution preparation and fiber electrospinning 38
5.1.2 Physico-mechanical properties and in vitro release behaviors of PLA/ASA fibers 41
5.1.2.1. Average fiber diameters 41
5.1.2.2. Average fiber mat densities 43
5.1.2.3. Mechanical properties 46
5.1.2.4. In vitro drug release assays 50
5.1.2.5. Fiber mechanical properties after drug releases 53
5.2. Hydrogen peroxide vapor calibration studies 57
5.2.1 Effects of liquid hydrogen peroxide concentrations 57
5.2.2 35% liquid hydrogen peroxide 61
5.3. Decontamination of Polylactic Acid Fibers 63
5.3.1. Fiber morphologies and fiber mat microstructures 63
5.3.2. Average fiber diameters 65
5.3.3. Physical Properties 67
5.3.4. Mechanical Properties 69
5.3.5. FTIR 74
5.3.6. Drug Release Assay 75

6 CONCLUSIONS AND SUGGESTED FUTURE WORKS 78

References 81

7

LIST OF FIGURES

Figure		Page
1	A schematic of electrospinning setup [45].	13
2	Explosion ranges of hydrogen peroxide [81]. (a) Explosion range of a combination of hydrogen peroxide and working solution. (b) Explosion range of hydrogen peroxide and TMB. (c) Explosion range of hydrogen peroxide and TOP.	23
3	Modified bubble machine for generation of hydrogen peroxide vapor.	33
4	The experimental setup of the materials compatibility studies using a glove box with the attachment of a hydrogen peroxide gas sensor. The bubble machine was placed inside the glove box with the fiber samples located at the furthest distance.	34
5	Scanning electron microscope images of electrospun PLA and PLA/ASA fibers on the effects of ASA stabilities in HFIP solvent, showing (a) blank PLA fibers (control groups), (b) PLA/ASA fibers (1 day), (c) PLA/ASA fibers (14 days), and (d) PLA/ASA fibers. Scale bar = 10μm.	39
6	Scanning electron microscope images of electrospun PLA and PLA/ASA fibers on the effects of ASA loadings, showing (a) blank PLA fibers (control groups), (b) PLA/ASA fibers (15%), (c) PLA/ASA fibers (30%), and (d) PLA/ASA fibers (45%). Scale bar = 10μm.	40
7	Average fiber diameters of electrospun blank PLA, PLA/ASA (1 day), PLA/ASA (14 days), and PLA/ASA (28 days) fibers (n = 30). An asterisk indicates statistical significance ($P < 0.05$).	41

8 Average fiber diameters of electrospun blank PLA, PLA/ASA (15%), PLA/ASA (30%), and PLA/ASA (45%) fibers (n = 30). An asterisk indicates statistical significance (P < 0.05). 42

9 Average fiber mat densities of blank PLA, PLA/ASA (1 day), PLA/ASA (14 days), and PLA/ASA (28 days) fibers (n = 3). An asterisk indicates statistical significance (P < 0.05). 44

10 Average fiber mat densities of blank PLA, PLA/ASA (15%), PLA/ASA (30%), and PLA/ASA (45%) fibers (n = 3). An asterisk indicates statistical significance (P < 0.05). 45

11 Tensile testing of blank PLA, PLA/ASA (1 day), PLA/ASA (14 days), and PLA/ASA (28 days) fibers, showing (a) representative stress strain curves, (b) average elastic moduli, (c) average tensile strengths, and (d) average elongation to failures (n = 4). 47

12 Tensile testing of blank PLA, PLA/ASA (15%), PLA/ASA (30%), and PLA/ASA (45%) fibers, showing (a) representative stress strain curves, (b) average elastic moduli, (c) average tensile strengths, and (d) average elongation to failures (n = 4). 50

13 Cumulative drug release profiles of PLA/ASA (1 day), PLA/ASA (14 days), and PLA/ASA (28 days) fibers (n = 3). 52

14 Cumulative drug release profiles of PLA/ASA (15%), PLA/ASA (30%), and PLA/ASA (45%) fibers (n = 3). 53

15 Mechanical properties of blank PLA fibers after degradation assays, showing (a) representative stress strain curves, (b) average elastic moduli, (c) average

tensile strengths, and (d) average elongation to failures for control, 2 hrs, and 48 hrs groups (n = 4). 54

16 Mechanical properties of ASA-loaded PLA fibers after drug release assays, showing (a) representative stress strain curves, (b) average elastic moduli, (c) average tensile strengths, and (d) average elongation to failures for control, 2 hrs, and 48 hrs groups (n = 4). 56

17 The effects of relative humidity (%) and Temperature (°C) on (a) 3.5%, (b) 10%, (c) 20%, and (d) 30% liquid hydrogen peroxide over 200 minutes inside the glove box. 59

18 Hydrogen peroxide vapor concentration profiles using 3.5%, 10%, 20%, and 30% of liquid hydrogen peroxide as the source for over 200 minutes inside a glove box. 60

19 Normalized relative humidity profiles using 3.5%, 10%, 20%, and 30% liquid hydrogen peroxide as the source for over 200 minutes inside the glove box. 61

20 Representative hydrogen peroxide vapor concentration and relative humidity profiles using 35% liquid hydrogen peroxide as the source for over 150 minutes inside the glove box. 62

21 SEM images of electrospun blank PLA fibers, showing (a) control fibers, (b) fibers after low level, (c) medium level, (d) high level of hydrogen peroxide vapor treatments using 35% liquid hydrogen peroxide as the source. Scale bar = 10 μm. 64

22 SEM images of electrospun ASA-loaded PLA fibers, showing (a) control fibers, (b) fibers after low level, (c) medium level, (d) high level of hydrogen

peroxide vapor treatments using 35% liquid hydrogen peroxide as the source. Scale bar = 10 μm. 65

23 Average fiber diameter of the blank PLA and ASA-loaded fibers after various levels of hydrogen peroxide vapor treatments using 35% liquid hydrogen peroxide as the source. 66

24 Percentage area change of the blank PLA and ASA-loaded PLA fibers after various levels of hydrogen peroxide vapor treatments using 35% liquid hydrogen peroxide as the source. 68

25 Percentage weight change of the blank PLA and ASA-loaded PLA fibers after various levels of hydrogen peroxide vapor treatments using 35% liquid hydrogen peroxide as the source. 69

26 Mechanical properties for blank PLA fibers, showing (a) representative stress strain curves, (b) average elastic moduli, (c) average tensile strength, and (d) average elongation to failure of the control, low, medium, and high level of hydrogen peroxide vapor treatment using 35% liquid hydrogen peroxide as the source. 71

27 Mechanical properties for ASA-loaded PLA fibers, showing (a) representative stress strain curves, (b) average elastic moduli, (c) average tensile strength, and (d) average elongation to failure of the control, low, medium, and high level of hydrogen peroxide vapor treatment using 35% liquid hydrogen peroxide as the source. 72

28 FTIR spectra of blank PLA fibers on the control, low, medium, and high level of hydrogen peroxide vapor treatments using 35% liquid hydrogen peroxide as the source. 75

29 In vitro drug release assays of PLA/ASA fibers from control, low, medium, and high level of hydrogen peroxide vapor treatments using 35% liquid hydrogen peroxide as the source. 77

Chapter 1

Introduction

1.1 Topical Drug Delivery

Topical therapies are one of the earliest medical treatments utilized by humans. Throughout the 20th and 21st centuries, the understanding of the behavior of drug carriers and their usage have advanced the topical drug delivery field rapidly due to the possibility to control the drug release rates [1]. Over the last few years, topical drug delivery has obtained increased attention from researchers due to its accessibility and their minimum systemic toxicity in treatment of local diseases [2].

Topical drug delivery is a method of treatment where the drug delivery system is applied to areas such as ophthalmic, rectal, vaginal, or skin to treat diseases and infections [2]. This non-invasive delivery system allows for an alternative route for drugs to be delivered to a specific site providing a more targeted treatment option [3]. There are many advantages in using a topical drug delivery system over the invasive drug delivery routes, including the improvement of drug bioavailability locally, the specific location of the drug being delivered, the easiness for the patients and healthcare to apply the drugs, and the long-term adherence on treatment plans due to patient compliance [4].

Various drug carriers have been investigated for the use of topical drug delivery systems, such as hydrogels, creams, gels, capsules, nanoparticles, and microfibers. Recently, electrospun microfibers receive an increased amount of attention in topical drug delivery systems due to a number of outstanding properties such as the ability to be made from a variety of polymers that can accommodate small molecule drugs and have a high surface area to volume ratio. First, electrospun microfibers can be made from a variety of polymers, where the choice of using a

natural polymer, a synthetic polymer, or a blend of both can be adjusted with the types of drugs that will be incorporated into the microfibers, allowing for flexibility in selecting the polymer. Second, electrospun microfibers can accommodate small molecule drugs with different physicochemical properties at a high loading (up to 60%) and a high encapsulation efficiency (up to 100%) for sustained drug delivery which is not always possible with other drug delivery systems [5]. Third, electrospun microfibers have a high surface area to volume ratio, which enables surface wetting to become a rate-limited step for the diffusion process of small molecule drugs. Finally, the requirements of sustained drug release behaviors for clinical applications can be tuned through the modifications of fiber diameters, fiber morphologies, fiber mat porosities, and/or drug loadings [6]. These outstanding properties such as flexibility in choosing the polymer, the ability to accommodate small molecule drugs, and the ability to maintain a sustained drug release through fiber modifications of electrospun fibers enable their uses in a variety of biomedical applications for controlled drug delivery.

1.2 Decontamination of the Drug delivery Systems

There are on average 53 million outpatient surgical procedures, and 46 million inpatient surgeries performed every year in the United States [7]. A major risk of all these procedures is the introduction of infection to the patient by failing to properly disinfect or sterilize equipment [7]. Hospital acquired infections (HAI) are considered the eighth most common cause of death in the United States [8]. These HAI can be transmitted through medical devices or the unclean hands of health care workers. There has been a substantial amount of evidence in recent years that contaminated surfaces contribute to the transmission of pathogens [9].

Dry cleaning, dusting, mopping, and using antibacterial wipes are some of the traditional cleaning methods that are used to clean biomedical devices. Dusting and dry cleaning can

disperse particles and spread microorganisms across surfaces. Mops can be used to clean large areas; however, there is a potential of spreading contamination to non-contaminated areas. Mops can be disinfected; however, the disinfecting process can degrade the effectiveness of mopping. Antibacterial wipes only achieve their maximum effectiveness when an elaborate procedure is followed, if the procedure is not followed it can increase the spreading of microorganisms [10]. Even by following procedures to ensure maximum effectiveness, traditional cleaning is not always enough to avoid a potential outbreak.

Decontamination of equipment and areas is needed to decrease the risk of disease and infection from spreading. Various approaches have been used to disinfect environments such as hospitals and laboratories, but there are many difficulties with material compatibility related to the equipment and surface areas in spaces [11]. Careful consideration is needed when determining the best option to perform decontamination on biomedical devices. Many biomedical devices are susceptible to moisture and heat, therefore different methods are needed when these devices are decontaminated to avoid the risk of HAI spreading among patients. Touch disinfectants, which are liquid disinfectants, are a common method used to disinfect equipment and areas that cannot be disinfected by heat. However, liquid disinfectants require that the object be submerged for a pre-determined amount of time. This requirement means the object cannot be susceptible to moisture or the equipment can be damaged [12]. Liquid disinfectants can be highly corrosive to certain materials such as metals and plastics when the items are disinfected. For example, chlorine dioxide or bleach has been found to be highly corrosive even to highly alloyed stainless steels [13]. Individuals who use liquid disinfectants are at a higher health hazard risk due to prolonged exposure while disinfecting items.

To avoid damaging equipment, non-touch disinfectants, which remove or reduce the reliance on operators with an improved efficacy at terminal disinfection [14], are an effective option when liquid disinfectants cannot be used. Non-touch disinfectants include UV light, ozone, and heat. These non-touch disinfectant methods are becoming more popular due to their ability to disinfect a wide variety of equipment and areas effectively. However, there are some drawbacks to the non-touch disinfectant methods such as they require a certain concentration of the decontaminant to contact all of the surfaces for a set amount of time in order to be effective and kill microorganisms [15]. One of the most popular non-touch disinfectants is vapor phase hydrogen peroxide (VHP) due to its effectiveness in killing microorganisms. However, when performing decontamination with VHP, safety is always a major concern. VHP can be hazardous to human health if the correct precautions are not followed. Even with short-term exposure, as low as 0.5-2 ppm, VHP can cause safety issues for the personnel using them [15]. In addition, potential leakages of VHP out of the area of decontamination can reduce its effectiveness [15]. Since each cycle of decontamination will have different requirements depending on the biomedical devices, considerations need to be taken into account for decision-making on the materials compatibility with VHP.

1.3 Thesis Hypothesis

In general, the purpose of this work is to: (1) study the drug stability in electrospun microfibers and the effects of drug loading on the physico-mechanical properties of the microfibers, and (2) determine the effects of vapor phase hydrogen peroxide on the physico-mechanical properties of drug-loaded electrospun microfibers. The hypothesis of the thesis is that drugs will be stable in the electrospun microfibers, whereas exposure of the microfibers to a hydrogen peroxide vapor environment will decrease the physico-mechanical properties and

produce a burst release behavior. The results from the thesis will provide significant information on the compatibility of electrospun drug-loaded microfibers after VHP treatments.

Although electrospun polylactic acid (PLA) microfibers have been extensively researched in the field of topical drug delivery, a case can be made that organic solvents and drug loadings affect drug stability in the fibers and their corresponding therapeutic performance. In the first part of the thesis, electrospun acetylsalicylic acid (ASA) - loaded PLA microfibers (15% loading) were produced after the drug/polymer solutions were mixed in hexafluoroisopropanol (HFIP) for 1 day, 14 days, and 28 days to determine drug stability in the organic solvent. After confirming the suitable mixing days for drug/polymer solution, electrospun ASA-loaded PLA microfibers were produced at 15%, 30%, and 45% ASA loading to determine the fiber physico-mechanical properties and in vitro drug release rates.

Vapor phase hydrogen peroxide has shown effectiveness and efficacy in decontamination; however, material compatibility has not been fully researched using electrospun drug-loaded microfibers. In the second part of the thesis, a portable H_2O_2 vapor generator and a H_2O_2 gas sensor were used to examine the effects of hydrogen peroxide vapor exposure on electrospun ASA-loaded PLA microfibers. Baseline studies on the relative humidity, temperatures, and hydrogen peroxide vapor concentrations were performed using liquid hydrogen peroxide of 3.5%, 10%, 20%, and 30% in an enclosed environment over a time period of 200 minutes. Furthermore, 35% liquid hydrogen peroxide was used to determine the three concentration-time levels at the plateau of the relative humidity and concentration. The effects of hydrogen peroxide vapor exposure on the fibers physico-mechanical properties and chemical structures were determined at various VHP treatment levels. In vitro drug release assay

was used to examine the effects of hydrogen peroxide vapor treatment conditions on the cumulative release of the ASA.

Chapter 2

Significance

The significance of this work is twofold: (1) to acquire a more comprehensive understanding on the effects of an organic solvent and drug loading on the physico-mechanical properties in electrospun microfibers and (2) to report the material compatibility of electrospun microfibers with vapor phase hydrogen peroxide. Drug stability and drug loading can play a significant role on drug release rates (e.g., increasing drug loading allows for a longer delivery period if the release rate is slow, which could reduce patient visits and improve patient compliance with the treatment). Therefore, drug delivery devices that contain high drug loading with slow release rates have gained interest from researchers over the past decade. In this area, limited research has been performed on drug stability in HFIP, one of the commonly used organic solvents, and how drug loading affects the physico-mechanical properties of the electrospun fibers.

During the process of electrospinning, there is a possibility of contaminating the fiber mat, thus, it might be necessary to sterilize the medical fabrics before administration topically. There are many sterilization methods, and vapor phase hydrogen peroxide decontamination has gained notability as a robust and effective disinfectant method across various industries. Although many research efforts have been taken place with examining the effects of vapor phase hydrogen peroxide on a material's physico-mechanical properties with industrial size decontamination units, there exists a fundamental question on how effective a handheld vapor phase hydrogen peroxide decontamination unit would be and its specific effects on electrospun microfibers.

Chapter 3

Literature Review

3.1 Drug Delivery Systems

Drug delivery systems (DDS) have played a key role in applications to deliver drugs for treatment of diseases and infections. In recent years, researchers have made advances and have developed various types of DDS to delivery drugs to a targeted area in the human body. These advancements improve local drug activities in the human body. Currently, various DDS such as nanoparticle, liposomes, hydrogels, scaffolds, and nanofibers have been developed.

3.1.1 Nanoparticles

Nanoparticles are particles having a diameter of 10-100 nm and are a common DDS. The advantages of using nanoparticles as a DDS include the improved drug efficacy, the increased drug half-life, the ability to perform controlled drug release, and the promotion of solubility for poorly water-soluble drugs [16]. Nanoparticles can be developed using either synthetic or natural polymers. Some synthetic polymers that are currently being used are polylactic acid (PLA) and poly(lactic-co-glycolic acid) (PLGA), while some natural polymers that are used include chitosan, gelatin and alginate [17]. To determine which type of natural or synthetic to use is dependent on the application of the DDS. Nanoparticles made of biodegradable polymers can also increase patient compliance to the treatment schedule due to sustained drug delivery [18]. Being made of the biodegradable polymers, it allows the nanoparticles to stay in circulation and in tissues for longer period of times than traditional methods. Barbieri et al. used tamoxifen-loaded lecithin-chitosan nanoparticles to increase the solubility and permeation of drugs across the intestinal epithelium [19]. Liu et al. used carboxymethyl chitosan nanoparticles as a carrier for carbamazepine (CBZ) to help treat epilepsy. This resulted in a faster absorption and also an

increase in the bioavailability of the drug crossing into the blood brain barrier. Through the use of nanoparticles, it also had enhanced brain targeting characteristics rather than the traditional method of antiepileptic drugs [20]. Pandey et al. used PLA nanoparticles to deliver tamoxifen (TMX) for breast cancer treatment. TMX showed an initial burst release with an approximately 65% being released in the first 24 hours, while approximately 80% after 4 days [21]. Householder et al. used PLGA nanoparticles to deliver hydrophobic payloads to an intracranial glioma. They encapsulated camptothecin (CPT) in the PLGA nanoparticles at 20 mg/kg drug loading. They showed that the nanoparticles could slow tumor growth and increase the rate of survival in comparison to other treatments [22].

3.1.2 Liposomes

Liposomes were the first nanoparticle-related DDS to be discovered [16]. Composed of phospholipids, either natural or synthetic, liposomes have a lipophilic tail and hydrophilic head on the same molecule. The hydrophobic tails make up the inner region of the membrane while a bilayer is formed due to the polar heads orientating themselves to the aqueous medium. Liposomes can improve drug efficacy, therapeutic index, and drug stability through drug encapsulation. They are also nontoxic, biocompatible and biodegradable [23]. Sonkar et al. loaded AuGSH (a diagnostic agent) into the core of the liposome while, DCX (a therapeutic agent) was loaded into the lipophilic bilayer to help improve brain targeted drug delivery. They managed to achieve a 70% drug loading for both the targeted and non-targeted formulation. They also demonstrated a slow and sustained release [24]. Huang et al. designed a biotin-glucose branched ligand-modified, dual-targeting liposomes. They significantly increased the number of liposomes in the breast tumor sites, which resulted in an increased tumor-targeting abilities [25].

3.1.3 Hydrogels

Hydrogels have been used for DDS for a long time. They have many definitions, however the most common definition used by researchers is a water-swollen and cross-linked polymeric network produced by the simple reaction of one or more monomers [26]. When drug-loading hydrogels come into contact with an aqueous medium, the hydrogel dissolved and releases the drug [27]. Hydrogels are an important area of study for drug delivery due to their wide range of application use from agriculture to biomedical engineering [28]. Due to their ability to absorb and retain large amounts of water, they are widely used in medicine and tissue engineering as they are similar to living tissue [29]. Sheu et al. used Doxorubicin (DOX) thermosensitive hydrogels incorporated with docetaxel (DOC)-loaded mixed micelles to deliver two drugs. They found that the hydrogels were thermosensitive, injectable, and capable of maintaining a sustained drug release. They determined that there was an increased efficacy of cancer chemotherapy. They also found that there was minimal side effects and a reduced chemoresistance [30]. Leach et al. developed an injectable hydrogel for release of cyclic dinucleotides (CDNs), which improved the survival in murine modal of head and neck cancer. It was also seen that an immunological memory was developed and rejected a secondary challenge of cancer cells in the surviving animals [31].

3.1.4 Scaffolds

Scaffolds play a key role in tissues engineering due to the fact that they can be an alternative to traditional implants of organs and tissues [32]. There are a few requirements when designing a scaffold. First, the scaffolds need to have a high porosity and high surface area. Second, the scaffolds need to be biodegradable and biocompatible. Lastly, the scaffolds must have the ability to maintain the mechanical integrity in the predesigned tissue structure. Patel et

al. used chitosan/cellulose nanocrystal scaffolds [33]. They found that composite scaffolds had improved the mechanical strength as well as the antibacterial activity. They also managed to maintain a sustained drug release.

A commonly used polymer for scaffold making is polylactic acid (PLA). This is due to its extra methyl group, which makes it more hydrophobic in comparison to other polymers such as polyglycolide (PGA), leading to a lower hydrolysis rate that other scaffolds [34]. Jadidi et al. developed a dual-functional scaffold for the purpose of bone tissue regeneration and local antibiotic delivery applications [35]. A bioresorbable bredigite scaffold loaded with vancomycin hydrochloride and was encapsulated in poly(lactic-co-glycolic acid) (PLGA) was developed. The scaffold improved the cell viability and the drug release by decreasing the burst release, which resulted in a sustained drug release. This showed the PLGA scaffold could be a viable option for osteomyelitis treatment. Cantón et al. showed that PLA/PLGA scaffold were able to release ibuprofen over a period of 160 hours [36]. There was an initial burst release and then slowed to a gradually release. The scaffold also degraded, which avoided the need to remove the dressing after treatment was completed.

3.1.5 Nanofibers

Nanofibers are fibers that have diameters ranging from tens of nanometers to a few micrometers. Nanofibers have high surface-to-volume (or weight) ratio, and they often have a porous structure and excellent pore interconnectivity [37]. Due to the small fiber diameter and large surface-to-volume ratio, nanofibers have demonstrated a significantly improved physical, chemical, and biological properties [38]. They are considered among one of the most universal and promising DDS. Nanofibers can be designed to possess a wide range of drug release behaviors and routes of administration not limited to but including oral, transdermal, and

transmucosal delivery [39]. Nanofibers are commonly made through the process of electrospinning. Hussein et al. electrospun coaxial nanofibers from blend polymers of polyvinyl alcohol (PVA) and polylactic acid (PLA) to delivery both Ag-chitosan nanoparticles and phenytoin [40]. They found that the nanofibers had an increase efficacy in both antibacterial and fibroblast proliferative properties than non-coaxial nanofibers. These fibers were promising for drug delivery in wound healing due to the improvement on the morphological, thermal, and mechanical properties of the fibers. Zahedi et al. electrospun PLA and polycaprolactone (PCL) fibers in a 50/50 blend with various doses of tetracycline hydrochloride, an antibiotic [41]. They found the nanofibers not only had a sustained and suitable drug release behavior, but also had an adequate water uptake, water permeability, and antibacterial activities. These nanofibers had a higher performance when compared to commercial wound dressing materials.

3.2 Electrospinning

To produce nanofibers, the process of electrospinning is performed. Figure *1* shows a set up for electrospinning. The process of electrospinning typically involves a syringe filled with a desired polymer solution that is connected to the positive end of a high voltage source. The negative end is then connected to the collector plate [42]. The syringe is placed into the syringe pump, which ejects the solution out at a specified flowrate, which is dependent on the solution in the syringe. The current flowing from the high voltage source charges the particles in the solution. This causes the particles to rapidly expand, forming a small and fine nanofiber at the tip of the needle. The nanofiber comes out of the needle tip whipping around, in what is called the whipping effect. This “spinning” characteristic that the fiber does, is concentrated into a small cone shaped area forming what is called a Taylor Cone [43]. An electric field is formed between the tip of the needle and the collector plate flowing in the direction towards the plate due to the

positive charge connected to the needle top and the negative connected to the collector plate. The fiber exits the needle tip and then travels across the electric field and makes contact with the plate. The fiber adheres to the surface of the wax paper and forms a fiber mesh attached to the plate over time. Some solutions are plagued with issues such as beading or a spraying effect. This occurs when a small bead at the tip of the needle, and that bead is carried across to the plate once it overcomes friction and a steady spray of tiny drops are carried across to the plate. These issues can normally be resolved through the adjustment of the electrospinning parameters. However, some polymers are more difficult to electrospin, thus they are plagued with a higher degree of beading or spraying due to their lower solution conductivity [44].

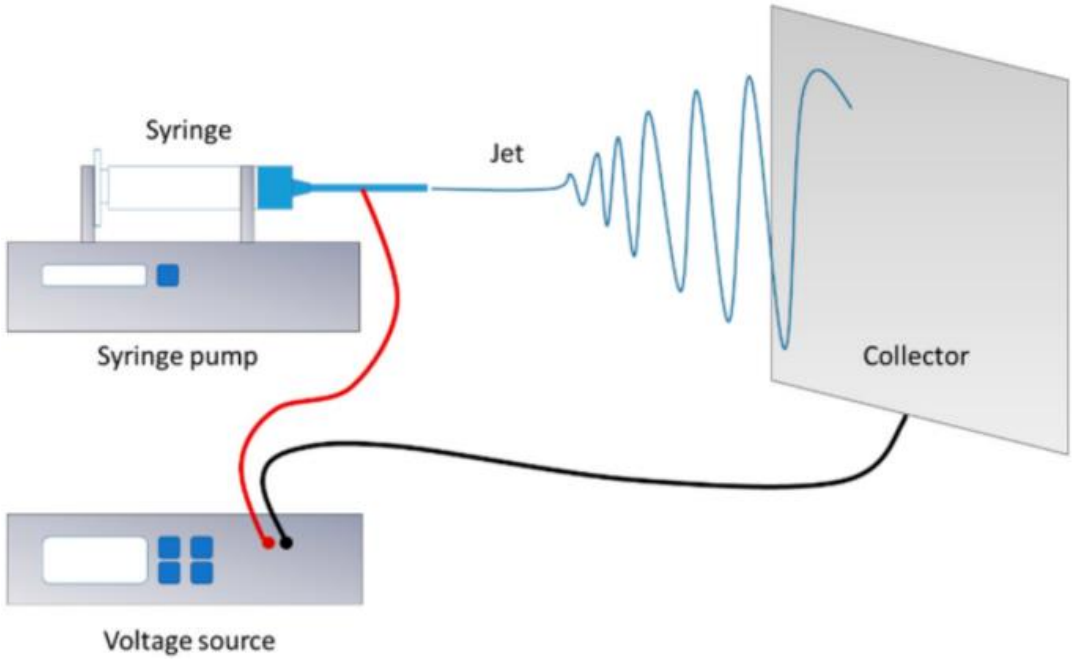

Figure 1. A schematic of electrospinning setup [45].

3.3 Polylactic Acid (PLA)

PLA is a widely used thermoplastic polyester derived from lactic acid. Since lactic acid is a constituent unit and a chiral molecule, it exists as two enantiomers, L- and D- lactic acid [46]. It can be used in a variety of applications such as tissue engineering, drug delivery systems, and various medical implants due to its ability to be used in scaffolds, films, nanoparticles and nanofibers [47,48]. A key point of PLA is its physical and chemical properties, which can be easily controlled, allowing researchers to obtain their desired properties. PLA is biodegradable and biocompatible, and it also has a high tensile strength and elastic modulus.

3.3.1 Degradation

PLA is degradable by a variety of mechanisms. These include and are not limited to, thermal, oxidative, and hydrolytic mechanisms [49]. The degradation rates of PLA is heavily influenced by a variety factors including humidity, oxygen, and the shape and size of the material [50,51].

3.3.1.1 Temperature

Thermal degradation of polymers leads to molecular deterioration. At higher temperatures the backbone of the polymer can break causing property changes to the polymer. Belbella et al. showed that the degradation process of PDLLA was increased with higher temperatures [52,53]. The results obtained were based on the amount of lactic acid released during the degradation as intra-molecular trans-esterification reaction led to cyclic oligomers of lactic acid and lactide. The PDLLA was observed after a month at three different temperatures, -18, 4 and 37°C. It was seen that the thermal degradation of PDLLA was faster at 37°C than at 4 and -18°C. Hyon et al. investigated long-term degradation behavior of PLLA fibers in PBS at 37 and 100°C [54]. It was found that the tensile strength was decreased to half of the initial strength

after 10 hours in PBS at 100 °C, while no change was found at 37°C. Overall, it can be seen that the degradation of PLA is dependent on the temperature. It should also be noted that the weight loss rate is drastically increased with temperatures that are higher than the glass transition temperature which is 63°C [55].

3.3.1.2 Oxidation

Thermal oxidation can take place throughout the material. It occurs when there is an interaction of oxygen at a high temperature with the material. As a result of oxidation, mechanical properties of material are reduced. It can also cause embrittlement of the material through the breaking of bonds [56]. Rasselet et al. has shown that oxidation affects the physical and mechanical properties of PLA [56]. Due to thermal oxidation, PLA experiences a decrease in molecular weight since the oxidation leads to a random chain scission process. Changes to the molar mass decreased the glass transition temperature while the degree of crystallinity was increased. It was also seen that strain at break was decreased due to the decrease in molar mass.

3.3.1.3 Hydrolytic

PLA degrades mainly through hydrolysis after a few months of moisture exposure. This degradation occurs in two stages. The first stage is the non-enzymatic chain scission of the ester groups which leads to a decrease in molecular weight. During the second stage the molecular weight is reduced until the lactic acid and low molecular weight oligomers are naturally metabolized by microorganisms. The decrease of molecular weight leads to a change in mechanical properties [57]. Tsuji et al. showed that tensile strength, Young's Modulus, and elongation-at-break decreased during hydrolysis [58]. PLLA films annealed at different temperatures were tested to evaluate the effect of hydrolysis on mechanical properties. As the

hydrolysis time increased there was a decrease in the mechanical properties, with a significant decrease between approximately 5 months to 12 months.

3.4 Decontamination Products

Many disinfectant products are available on the market, ranging from touch disinfectants, which include liquid disinfectants, to non-touch disinfectants. These products can disinfectant the surfaces and items that are used in daily life and highly specialized equipment such as medical devices.

3.4.1 Contact Disinfectants

Various chemicals are used to disinfect items and environments that cannot be disinfected through other methods such as thermal disinfecting. However, a major drawback to using liquid disinfectants is that the item needs to be fully submerged for a period of time. Thus, the item needs to be liquid proof to kill any microorganism without damaging the item.

3.4.1.1 Sodium Hypochlorite

Sodium hypochlorite, more commonly known as bleach, is a widely used and accessible product. It is used to disinfect equipment, surfaces and even laundry. It is a strong oxidizing agent with a broad-spectrum antimicrobial effect and is classed as a low or intermediate level disinfectant depending on the concentration level. The effectiveness of sodium hypochlorite is highly dependent on the amount of organic load. It is highly effective in dealing with blood spillage and decreasing the risk of transmission of viruses. It impairs bacterial oxidation by releasing chlorine which damages the bacterial cell walls. Bacteria can be killed within 1 minute, and fungi and viruses are extremely susceptible. However, it can be corrosive to metals, certain plastics and fabrics depending on the concentration. It also needs to be thoroughly removed after it is used. Rios-Castillo et al. used different sodium hypochlorite disinfectants to determine its

short- and long-term decontamination efficacy on *Staphylococcus aureus* and *Enterococcus hirae*, which are two common bacterium found in the food industry [59]. It was seen that the disinfectants were most effective in the short term, while their long-term disinfectant ability was ineffective after 24 hours. Tiwari et al. also found success in the effectiveness in reducing the viable bacteria [60].

3.4.1.2 Alcohol

Alcohol is a widely used disinfectant typically found in the form of ethyl or isopropyl alcohol, which are water-soluble compounds. The effectiveness is dependent on the concentration of the alcohol, and it is most active when used at concentrations between 60 and 90%. When diluted below 50%, their anti-bacterial efficacy drops dramatically. Microbial death occurs from protein coagulation and denaturing of the membrane protein [12]. Alcohol is useful in disinfecting medical equipment such as thermometers and stethoscopes. It is also beneficial in disinfecting horizontal surfaces due to alcohols fast evaporation leaving surfaces dry after its use. Due to its flammability, alcohol needs to be stored properly [61]. Jury et al. found that Biomist, an alcohol disinfecting system, was capable of significantly reducing the contamination of methicillin-resistant *Staphylococcus aureus* (MRSA) and vancomycin-resistant enterococci (VRE) on commonly touched surfaces in rooms that housed MRSA infected patients [62]. It was also found that Biomist was easy to use and required no more time to disinfect when compared with standard cleaning agents.

3.4.1.3 Glutaraldehyde

Glutaraldehyde is a rapid disinfectant when used to kill vegetative bacteria and viruses yet is slowly effective against spores and mycobacterium. It is used as a high-level disinfectant on medical equipment. Glutaraldehyde works by denaturing cell proteins [12]. When an

alkalinizing agent is added to glutaraldehyde, the solution becomes sporicidal. It has advantages over other disinfectant as it is relatively inexpensive and has excellent material compatibility. However, it can cause respiratory irritation and is highly toxic. It also attaches tissue and blood to surfaces [7]. Best et al. showed that less than 6-log reduction was achieved when used against *S. aureus* [63].

3.4.2 Non-contact Disinfectants

The effectiveness of touch disinfectants is limited by the human operator ability to choose the correct disinfectant and to clean all the necessary surfaces. Non-touch disinfectants allow for the elimination of a human operator to clean all the surfaces. They also can be used when conventional touch disinfectants cannot be used. These methods have become more popular due to their advantage in decontaminating a wide variety of equipment's and areas.

3.4.2.1 Ozone

Ozone is a powerful tool against bacteria, fungi, protozoa, and viruses due to its oxidizing capacity. Through oxidation, ozone attacks the wall and membranes of microbial cells, and it also alters the cell permeability. A drawback of using ozone as a disinfectant is that it is very unstable and must be generated in the area needed to be disinfected. It is also very toxic to humans, and a concentration of 1 ppm can cause chest pain, coughing, and shortness of breath. However, it has environmentally friendly by-products as it decomposes into oxygen [64,65]. The effectiveness of ozone was tested using *Escherichia coli* and *Staphylococcus aureus* [66]. Ozone at concentrations between 300 and 1500 ppm were used for 10-480 seconds, and a death rate above 99.99% was achieved on both bacteria.

3.4.2.2 Chlorine-releasing Agents

As a bactericide, fungicide, virucide, and algicide, chlorine dioxide is a powerful disinfectant. Chlorine dioxide achieves its disinfecting abilities through the oxidation of sulfhydryl (SH) groups on proteins that are essential to cells [67]. It is widely used to disinfect drinking water, poultry processing water, and fruits, and vegetables. Additionally, there is no bacteria that is known to be resistant to chlorine dioxide. However, chlorine dioxide gas can cause eye, skin, and respiratory irritation [68]. It can also be corrosive to steel surfaces. Since it is a hazardous gas, it needs to be produced on site. It has been shown that concentrations as low as 2 mg/L can inactive greater than 5-log CFU/cm^2 of *Listeria monocytogenes* biofilm cells [67,69]. Ahned et al. showed that 6 hours have the highest disinfection rate of *E. Coli* in comparison to 10 minutes, 1, 3, and 12 hours when using 250 mL of chlorine dioxide gas [70].

3.4.2.3 UV Light

UV light is in the section of the electromagnetic spectrum that has wavelengths 100-400 nm. Between 100-280 nm wavelength range, UV light has germicidal properties. This is due to the DNA mutations that occur when the light is absorbed. It damages the DNA by stopping their ability to replicate [71,72]. UV Light can be applied in two different ways, in a continuous or pulsed form. High levels of microbial inactivation can be achieved with UV light. However, exposure to UV light can lead to cancer, suppress the body's immune system, and can cause eye damage. It can also have poor penetrative power which could lead to microorganisms being shielded by soil. Chauret et al. showed that inactivation of 6-log of *E. coli* O157:H7 and *Listeria monocytogenes* could be achieved [69].

3.5 Hydrogen Peroxide

3.5.1 Process

Four key steps are involved in the operational cycle for the optimal generation of hydrogen peroxide vapor. They include: vaporization, gas concentration, micro-condensation formation, and re-evaporation. During the first step, liquid is vaporized into small molecules until it meets the target volume. The second step involves in developing the gas conditions in the environment to achieve saturated vapor conditions. This step is heavily dependent on the humidity and the surface temperature within the area. The third step is when a layer of micro-condensation forms on the surfaces. Lastly, the fourth step is the re-evaporation of the condensation and removal of the residual gas until a safe level is attained. The last step is primarily for safety [73].

Four main phases are in a typical vaporized hydrogen peroxide decontamination cycle. They include: Dehumidification, conditioning, decontamination, and aeration. In the first phase, the relative humidity is reduced to approximately 30-40% through the circulation of sterile air in a closed loop. By reducing the relative humidity, the vapor hydrogen peroxide is prevented from condensing out and allows it to operate at its most effective state. In the second phase, the decontaminant is produced through the process of vaporization until a desired concentration is achieved through a vapor phase hydrogen peroxide generator. The third phase involves the continuous injection of hydrogen peroxide and a certain recirculation flow rate to maintain the target concentration. This phase is carried out for the desired exposure time. Lastly, during the aeration phase hydrogen peroxide is no longer introduced. Residual vapor is safely decomposed into water and oxygen through a chemical destroyer. This phase is continued until the vapor

concentrations have been reduced to an acceptable level. The chemical destroyer is used to reduce the length of time of this phase [73,74].

3.5.2 Safety

The effects that hydrogen peroxide have on humans vary largely depending on the concentration. Hydrogen peroxide can be toxic if ingested, inhaled or through contact of the skin or eyes. The concentration of hydrogen peroxide that can be typically bought in supermarkets is approximately 3%. At 3%, inhalation can cause respiratory irritation and ingestion could result in vomiting and mild gastrointestinal irritation. Exposure can cause mild ocular irritation; severe injuries are rare. Skin contact can cause irritation and temporary bleaching of the skin and hair at 3%. At concentrations between 10-20%, ingestion has similar symptoms as the lower concentration, but exposed tissues may also be burned. Inhalation of vapors of concentrations higher than 10% may result severe pulmonary irritation. Exposure can result in perforation or ulceration of the cornea. At concentrations greater than 20%, ingestion can lead to rapid loss of consciousness followed by respiratory paralysis. Skin contact could cause severe burns with blisters. Ernstgård et al. conducted a study to evaluate the acute effects of low concentration of hydrogen peroxide on humans [75,76]. Volunteers were exposed to 0 ppm, 0.5 ppm, and 2.2 ppm of hydrogen peroxide for 2 hours at rest. The results showed nasal and throat irritation were increased slightly at 2.2 ppm but not at 0.5 ppm and 0 ppm. Lastly, no exposure-related effects were seen on blinking frequency, breathing frequency, pulmonary function, or nasal swelling. This suggests that at 2.2 ppm, hydrogen peroxide is slightly irritating.

3.5.3 Potential Dangers

The main safety hazard in using hydrogen peroxide is associated with heating. When hydrogen peroxide is heated, it undergoes a process of chemical decomposition, resulting in a

decreased stability. Hydrogen peroxide decomposes into its respective components of hydrogen and oxygen, or more specifically it decomposes into water and oxygen. The decomposition into oxygen is especially emphasized when talking about safety hazards. The release of oxygen could result in an explosion due to the buildup of pressure if the hydrogen peroxide was stored in a confined space. Additionally, pure oxygen is extremely flammable, and therefore due to this the oxygen produced needs to be properly ventilated to ensure that no spark can be found near the resulting oxygen.

Hydrogen peroxide with concentration levels of 74% or higher can create ignitable vapors. However, caution should be taken for concentration lower than 74%. It is highly recommended to avoid mixing high concentrations of hydrogen peroxide with fire due to flammability or other oxidizing agents due to the potential safety hazards [77–79]. Gomez Garcia et al. conducted experiments to assess the thermal safety for the decomposition of hydrogen peroxide through the utilization of dynamic analysis [80]. Bifurcation and continuity diagrams were mapped, and different thermal steady states were identified. It was found that the thermal cyclical behavior was the most predominant dynamic state of the reactive system.

Another insightful study analyzing the safety hazards of vaporized hydrogen peroxide was conducted by Jia et al. where explosive characteristics of mixtures containing hydrogen peroxide were explored [81]. This was investigated through the use of a drop weight test, and the explosion range was interpreted by thermal calculations and compared with the experimental results of the drop weight test. The explosion ranges can be seen represented in the diagrams below. In Figure *2*a, a combination of hydrogen peroxide and working solutions was used. The mixture for Figure *2*b consisted of hydrogen peroxide and TMB (1,3,5-trimethyl benzene). Finally, in Figure *2*c the mixture contained hydrogen peroxide and TOP (trioctylphosphate). The

calculated results agreed with the experimental results determined by the drop weight test. It was determined that the explosion range of the working solution/hydrogen peroxide mixture with surfactant was significantly larger than the mixture without it. It was concluded that the addition of the surfactant made the contact area of the mixture larger which resulted in a more violent reaction.

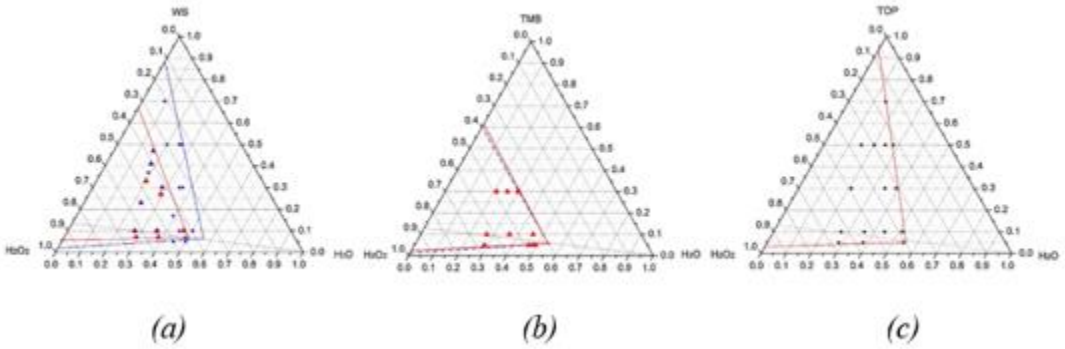

Figure 2. Explosion ranges of hydrogen peroxide [81]. (a) Explosion range of a combination of hydrogen peroxide and working solution. (b) Explosion range of hydrogen peroxide and TMB. (c) Explosion range of hydrogen peroxide and TOP.

3.5.4 Material Compatibility

Material compatibility when using hydrogen peroxide is a big concern for researchers. Due to hydrogen peroxide's corrosiveness and oxidative properties, the effect it will have on materials has been intensively studied.

3.5.4.1 Metal

Hydrogen peroxide is a useful disinfectant to be used around metal. However, consideration needs to be taken into account that most structural supports for buildings and airplanes are constructed of metals. The damage of these structures will increase the probability

of fracture or breaking and could lead to the loss of human lives. The key properties to focus on to guarantee structures stay standing are the microstructure, tensile properties, and corrosion resistance. Gale et al. experimented on type 304 austenitic stainless steel and age-hardened aluminum alloys 2024 and 7075 and examined the 3 key properties [82]. There was no changed observed in the bulk composition or the microstructure. There was also little to no change observed in the surface softening and was confined to the immediate surface of the materials. There was negligible weight changes, when expose to one cycle of VHP, although after 25 cycles there was a small weight change which is assumed to be due to oxidation of the metals.

3.5.4.2 Polymers

Careful consideration needs to be taken when using VHP on polymer fabric due to the increased chance that the fibers might become oxidized by the hydrogen peroxide. Oxidation of the fibers would, not only result in a decrease in mechanical strength but also increase the chance to absorb the atmospheric moisture prior to the decontamination stage. This absorption would affect the rate of oxidation of the polymer structure throughout the VHP process. Finally, it is a safety concern as the residual hydrogen peroxide can cause health related issues for individuals who might come into contact with the fibers. Chou et al. performed experiments using a VHP device to determine the compatibility of commonly used fabrics in aviation [83]. It was found that wool, nylon, polyester, and Nomex® had an increase of weight. This is assumed to be due to the absorption of water during the VHP treatment and then by-products during the aeration stage. Leather samples experienced a net loss of weight after VHP treatment. The tensile strength of wool, leather, polyester, and nylon all experienced a decrease. Wool's tensile strength had a 20-30% loss, which with the longer of exposure to hydrogen peroxide. The leather experienced a

50% loss in tensile strength after VHP exposure. Polyester and nylon experienced slight degradation, approximately 10% with minimum degradation and less than 10% respectively.

Many historical items made of fabric are extremely susceptible to destruction by microorganisms that come from soil, air, and water. These microorganisms can lead to changes in color and even changes in the physical properties of the objects. Anna et al. tested clothes and suitcases that were on display in Auschwitz-Birkenau State Museum that had low to medium levels of microbial contamination [84]. Through disinfection with VHP, it was found that the color of the historical cotton fabric, the chemical composition, and the morphology of the degree of cellulose polymerization were not changed to an extent that would have been deemed unacceptable by the conservators of the fabrics. It was recommended that the decision to disinfect historical items should be determined by conservators after the analysis of the items as VHP has different effects on various materials.

3.5.4.3 Composite Materials

Composite materials are used widely throughout many electronic components. Loo et al. conducted an experiment to determine the effects of VHP on electronic avionic materials [85]. It was found that VHP had no effect on the circuit boards, and no statistical difference could be found when analyzing the resistance and impedance readings. Results also indicated that there was no statistical change in weight and no degradation or oxidization chemically occurred between the boards and wires that were exposed to VHP. It was shown that the wires failed quicker on average after being exposed to VHP, however these tests were conducted with voltages that were higher than realistic voltage levels.

3.5.5 Efficacy

VHP systems are used extensively throughout the medical field from disinfecting equipment to rooms that have been used to treat and house patients who have highly contagious diseases. This is because hydrogen peroxide produces both a hydroxyl (OH) and hydroperoxyl (OOH) functional groups. The cell walls of microorganism are targeted and attacked by the hydroxyl and hydroperoxyl functional groups, thus destroying the microorganism.

To maximize the effectiveness of vaporized hydrogen peroxide as a disinfectant, a high concentration of liquid hydrogen peroxide needs to be converted into a vapor form without decomposition occurring. Moreover, the gas concentration needed for a target area is dependent on the humidity and the minimum surface temperature in the target area. Ideally, the delivered vapor achieves micro-condensation to form a micro-layer of disinfectant to destroy microorganisms. Lastly hydrogen peroxide vapor is required to be removed from the target area until a safe level is achieved [73,86].

Barbut et al. used vaporized hydrogen peroxide in a hospital room to test the effectiveness of the vapor [87–89]. They found that the HPV system achieves a greater than 6-log reduction on *C. difficile* spore in vitro, and further testing showed a complete eradication of *C. difficile* on hospital surfaces. These results were verified using 6-log *Geobacillus stearothermophilus* biological indicators. When compared to the other systems used, the HPV achieved up to a 4-log and the UV achieved up to 3-log on *C. difficile* spores in vitro, where neither of these systems could completely eradicate *C. difficile* on hospital surfaces. To achieve the log reduction in the hydrogen peroxide vapor or HPV decontamination, 30% liquid hydrogen peroxide was injected into a room for 15 minutes until a dose of 8 g/m^3 until hydrogen peroxide was covering all exposing surfaces. After 15 minutes contact time, the HPV was converted to

oxygen and water vapor. The total time required for the entire process was approximately 90 minutes. Fu et al. were able to achieve a greater than 6 log reduction in 9 out of 11, 6 out of 11 and all locations against MRSA, *A. baumannii*, and *C. difficile*, respectively. The HPV system in Fu et al. study also used 30% liquid hydrogen peroxide, but a concentration of $10g/m^3$ was recommended [79,89–98]

Chapter 4

Materials and Methods

4.1 Materials

Polylactic acid (PLA) was purchased from PolySciTech®, Akina Inc. (West Lafayette, IN, USA) with an average molecular weight (M_w) of 100 ~ 125 kDa. Hexafluoroisopropanol (HFIP) was purchased from Richest Group Ltd. (Shanghai, China). Acetylsalicylic acid (ASA) and phosphate-buffered saline (PBS) buffer solution (pH ~ 7.4) was purchased from Avantor (Radnor, PA, USA). All other chemicals were of reagent grade and used as received without further purification.

4.2 Preparation of polymer solutions

PLA solutions were prepared by dissolving PLA in HFIP. Briefly, masses of the PLA pellets were measured using a Mettler Toledo AG245 analytical balance (Columbus, OH, USA), whereas the corresponding volumetric amounts of HFIP were dispensed into glass vials using a micropipette (resolution = 0.1 μL) to achieve 15% (w/v) of PLA in HFIP. The 15% of PLA was chosen in accordance with other studies in literature [99–102]. The glass vials were placed on a Thermo Scientific™ Labquake™ rotisserie mixer (Waltham, MA, USA) for dissolution of PLA in HFIP at room temperature overnight.

For preparations of PLA/ASA solutions on the effects of ASA mixing days in HFIP, predetermined amount of ASA was measured at 15% (w/w: ASA/total polymer) and added into the PLA solution. PLA/ASA solutions were then further mixed on the rotisserie mixer for 1 day, 14 days, and 28 days, corresponding to the sample names of PLA/ASA (1 day), PLA/ASA (14 days), and PLA/ASA (28 days), respectively.

For preparations of PLA/ASA solutions on the effects of ASA loadings in PLA fibers, predetermined amount of ASA was measured at 15%, 30%, and 45% (w/w: ASA/total polymer) and added into the PLA solution 1 day prior to electrospinning. Samples were labeled as PLA/ASA (15%), PLA/ASA (30%), and PLA/ASA (45%), corresponding to each drug loading capacity in the PLA fibers, respectively. These drug loadings were chosen to study their effects on fiber physico-mechanical properties [103,104].

4.3 Electrospinning of PLA/ASA fibers

All polymer solutions were visually examined with care for undissolved particles prior to electrospinning. Polymer solution was drawn into a 3-mL BD Luer-lock^{TM} disposable syringe (Franklin Lakes, NJ, USA) that was attached to a 21-G blunt needle. The syringe and needle assembly were placed onto a NE-1000 programmable single syringe pump (Farmingdale, NY, USA). The syringe pump was calibrated to a diameter of 8.725 mm for the 3-mL BD syringe to dispense polymer solution at a flow rate of 20 μL/min. During electrospinning, a total of 3-mL of the polymer solution, recorded by the programmable pump, was dispensed through an applied voltage at around 10 kV with a deposition distance of 10 cm. Fibers were collected on a grounded stationary collector plate that was covered with a layer of wax paper. After each electrospinning, fiber sheets were covered with additional wax papers and stored in a vacuum desiccator to evacuate the organic solvent prior to fiber characterizations

4.4 Characterizations of electrospun fibers

Electrospun blank and ASA-loaded PLA fibers were characterized by fiber morphology to inform drug stability and drug loading capacity. The fiber physico-mechanical properties were correlated using mechanical tests, fiber diameters, fiber mat density and in vitro drug release assays.

4.4.1 Fiber morphologies

The morphologies of the electrospun blank and ASA-loaded PLA fibers were evaluated using a scanning electron microscope (SEM). Circular disk punches of the fiber meshes were placed on the carbon tape for imaging. SEM images were captured using a Hitachi TM4000Plus System (Tokyo, Japan) at 15kV with a working distance of approximately 5.5 ~ 6.0 mm.

4.4.2 Fiber diameters

Average fiber diameters were measured using the ImageJ software, National Institutes of Health (Bethesda, MD, USA), on the collected SEM images. Specifically, 30 random measurements were taken from SEM micrographs to determine the average fibers diameter and the standard deviations of each sample (n = 30).

4.4.3 Fiber mat densities

Average fiber mat densities were determined using the apparent density method. Specifically, masses of the fiber discs were measured using a Mettler Toledo AG245 (Columbus, OH, USA) analytical balance. Volumes of the fiber discs were determined using a digital thickness gauge (resolution = 10 μm) and area measurements from ImageJ software, National Institutes of Health (Bethesda, MD, USA). Three measurements were taken from samples to determine the average fiber mat density and the standard deviation of each sample (n = 3).

4.4.4 Mechanical testing

Dog-bone tensile specimens of 22 mm in nominal length and 5 mm in width according to ASTM D1708-96 [105] were punched from the fiber mats using an ODC stainless steel die (Waterloo ON, Canada). The thickness of each sample at the nominal region was measured using a digital thickness gauge (resolution = 10 μm).

A single column screw-driven Instron® 3342 universal material tester (Norwood, MA, USA) was used to perform uniaxial tensile tests. During the tests, a strain rate of 0.01/s was applied to the specimen, whereas the corresponding loads at timepoints were recorded using a 100 N load cell under 23 ± 2 °C and 50 ± 5% RH in accordance with ASTM D882-18 [106]. The recorded load and displacement data from the instrument were used to calculate the stress-strain curve of each sample. Young's modulus (slope of the initial linear region), tensile strength (zero slope or the highest stress), and elongation to failure (fracture strain) were determined from the corresponding stress-strain curve of each sample in Microsoft Excel (Redmond, WA, USA) (n = 4).

4.4.5 In vitro drug release studies

Circular discs of 7/16" in diameter were taken from each of the PLA/ASA fiber mat for in vitro drug release studies. Masses of fiber discs were measured to determine the corresponding volumes of the release media of phosphate-buffered saline solution (PBS) (pH ~ 7.4) based on the ASA standard curve. Glass vials containing predetermined amount of PBS were placed into a Thermo Scientific™ MaxQ 4450 orbital shaker (Waltham, MA, USA) prewarmed to 37 °C at 120 rpm.

A 40-µL liquid sample, containing unknown ASA concentration, was removed from each glass vial and placed in a 1.5 mL cuvette using a clean pipette tip for each extraction at predetermined time points of 1, 2, 4, 8, 24, and 48 hours. After each extraction of the sample vials, a 40-µL of fresh PBS was pipetted into each glass vial to replace the extraction volume to ensure consistent volume of the total release media.

ASA standard solutions were prepared via serial dilation methods (i.e., 400, 200, 100, 50, and 25 ppm) in PBS. Both the standard ASA solutions and the unknown ASA liquid specimens

collected at various time points were analyzed using a Thermo Scientific™ NanoDrop™ 1000 UV-Vis spectrophotometer (Waltham, MA, USA) at 231 nm and 298 nm. The initiation process of the UV-Vis measurement included cleaning of the pedestals using 95% ethanol followed by a background detecting of the release media for calibration. The resulting intensities of ASA at 231 nm and 298 nm from the unknown samples of various released time points were compared to the standard ASA curves to determine the in vitro cumulative release rate of ASA. Results were average on three independent measurements (n = 3).

4.5 Handheld hydrogen peroxide device

Concentrated liquid hydrogen peroxide (35%) was purchased from Avantor (Radnor PA, USA) as the source to produce hydrogen peroxide vapor. An iTeknic bubble machine was purchased from Amazon (Seattle, WA, USA) to represent a small handheld hydrogen peroxide vapor device. The bubble machine was modified to allow for the most efficient hydrogen peroxide delivery. Modifications of the bubble machine included the removal of the bubble wands from the bubble machine to allow the placement for a Protec® wicking filter purchased from Amazon (Seattle, WA, USA) into the liquid compartment of the bubble machine. This allowed for the liquid hydrogen peroxide to be soaked up and dispersed out in the vapor form. Figure *3* shows the setup of the bubble machine.

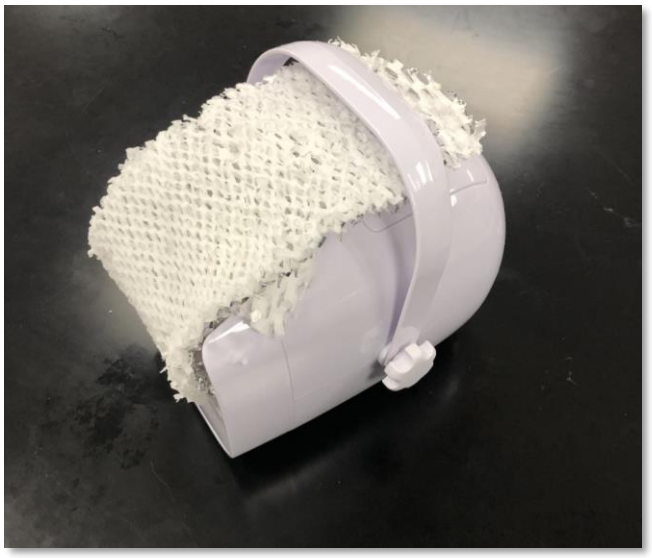

Figure 3. Modified bubble machine for generation of hydrogen peroxide vapor.

4.6 Hydrogen peroxide vapor calibration

In order to conduct the calibration experiments on hydrogen peroxide vapor, a glove box was purchased from Scienceware (Warminster, PA, USA). This allowed for the control of humidity and the concentration throughout the experiment. To monitor the hydrogen peroxide concentration, a PortaSens III Portable Gas Leak Detector Model D16 hydrogen peroxide vapor sensor was purchased from Analytical Technologies (Collegeville, PA, USA). To monitor the humidity, an AcuRite humidity sensor (Lake Geneva, WI, USA) was used.

All the calibration runs were performed inside of the glove box, which allowed for a control environment to conduct the calibration process. The glove box had an opening that allowed for the placement of items inside. This opening was later sealed to provide a controlled environment. There were two valves located on the backside of the glove box. A hose was attached to one of the valves to allow for the concentration of hydrogen peroxide to be measured inside the glove box. At the end of the calibration, both of these valves are opened to allow for

the dispersion of hydrogen peroxide vapor inside the glove box. Figure *4* shows the setup of the glove box.

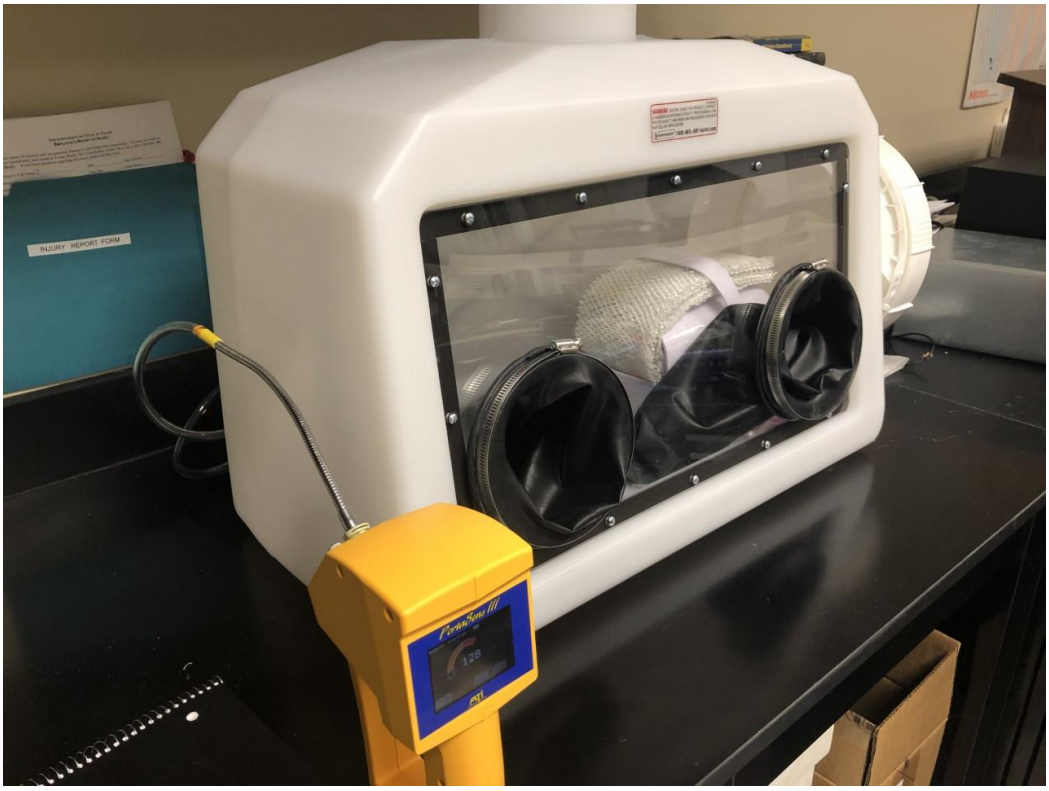

Figure 4. The experimental setup of the materials compatibility studies using a glove box with the attachment of a hydrogen peroxide gas sensor. The bubble machine was placed inside the glove box with the fiber samples located at the furthest distance.

Prior to performing hydrogen peroxide vapor exposure experiments on the polylactic acid (PLA) fiber samples, hydrogen peroxide vapor calibration runs were performed to evaluate the effectiveness on the setup of the handheld device. In brief, the bubble machine was placed inside the glove box allowing the measurement of hydrogen peroxide vapor concentration and humidity using the hydrogen peroxide vapor sensor and the humidity sensor, respectively. The calibration runs were performed to determine if the device would efficiently produce hydrogen peroxide

vapor and to determine when the relative humidity and hydrogen peroxide vapor concentration would plateau. The concentration and humidity of the hydrogen peroxide calibration runs were recorded over 200 minutes to determine the plateau. The device was placed inside the glove box, as well as the humidity sensor. The liquid hydrogen peroxide was diluted to 3.5% v/v, 10% v/v, 20% v/v and 30% v/v to examine the effects of hydrogen peroxide vapor concentration. The data was analyzed using one phase association to determine the plateau and the rate constant.

4.7 Hydrogen peroxide vapor exposures on PLA fibers

The experimental setup involved a glove box, bubble machine, humidity reader, and a hydrogen peroxide vapor sensor. A hose was attached to the back of the glove box to allow for the monitoring of the hydrogen peroxide vapor concentration. The humidity reader and bubble machine were placed inside the glove box. The fibers samples were placed in Ziploc bags to allow for accurate determination of the hydrogen peroxide vapor exposure concentration-time level. Once the samples were placed in the glove box, the box was closed to allow for a sealed environment. The bubble machine was then turned on. The hydrogen peroxide vapor concentration and humidity were monitored to achieve the parameters necessary to perform materials compatibility studies. The humidity ranged between 75%-95% and the concentration-time levels were 10,800 ppm-min, 32,400 ppm-min, and 54,000 ppm-min, which were named as low, medium, and high groups, respectively.

4.8 PLA/ASA fibers after hydrogen peroxide vapor exposures

Electrospun PLA/ASA fibers after undergoing hydrogen peroxide vapor exposures of low, medium, and high concentration-time level were characterized by fiber morphology to inform the effects of hydrogen peroxide vapor on the mechanical properties as well as fiber

diameters, area and weight change, and in vitro drug release rates to correlate fiber physico-mechanical properties.

4.8.1 Fiber Morphology

Similar to Section 4.4.1, the fiber morphologies of blank PLA and PLA/ASA fibers after exposing to low, medium, and high levels of hydrogen peroxide vapor were evaluated using a scanning electron microscope (SEM). Circular disk punches were placed on carbon tape for imagining. SEM images were captured using a Hitachi TM4000Plus System at 15kV with a working distance if approximately 5.5 ~ 6.0 mm.

4.8.2 Fiber Diameter

Similar to Section 4.4.2, the average fiber diameters were measured using the ImageJ software on the collected SEM images. Specifically, 30 random measurements were taken from SEM micrographs to determine the average fiber diameter

4.8.3 Weight Change

Average percentage weight change of PLA fibers was determined using a Mettler Toledo AG245 (Columbus, OH, USA) analytical balance. The samples were weighed before and after exposure of low, medium, and high level of hydrogen peroxide vapor, respectively. Three measurements were taken from each sample group to determine the average weight change and standard deviation (n = 3).

4.8.4 Area Change

Average percentage area change of PLA fibers was determined using an HP Deskjet 2540 (Palo Alto, CA, USA) and ImageJ software, National Institutes of Health (Bethesda, MD, USA). Circular disk punches of ½” diameters were used. The area was recorded for each sample before and exposure of low, medium, and high level of hydrogen peroxide vapor, respectively. Three

measurements were taken from samples to determine the average area change and standard deviation (n = 3).

4.8.5 Mechanical Testing

Similar to Section 4.4.4, mechanical testing on the blank PLA and PLA/ASA fiber specimens, dog-bone samples after exposure of low, medium, and high level of hydrogen peroxide vapor were used for uniaxial tensile tests on the Instron® 3342 universal materials tester (Norwood, MA, USA). The applied strain rate was 0.01/s, and the corresponding load and displacement data were transferred to Microsoft Excel (Redmond, WA, USA) for calculation of the mechanical properties.

4.8.6 Fourier-Transform Infrared Spectroscopy (FTIR)

The chemical structure of the blank PLA fibers after low, medium, and high level exposure of hydrogen peroxide vapor was analyzed using a Thermo Fisher Scientific Nicolet iS10 ATR-FTIR spectrophotometer (Walthem, MA, USA). The spectra were collected between 4000 and 600 cm^{-1} with a resolution of 8 cm^{-1}. Information for the peaks of the samples was obtained using OMNIC™ software.

4.8.7 In vitro Drug Release Assay

Similar to Section 4.4.5, 7/16” circular fiber discs were taken from each of the blank PLA and PLA/ASA fibers after low, medium and high level of exposure to hydrogen peroxide vapor for in vitro drug release studies. Masses of the fiber discs were measured to determine the corresponding volume of the release media of phosphate-buffered saline solution (PBS) (pH ~ 7.4) based on the ASA standard curve. Glass vials containing predetermined amounts of PBS were placed in a Thermo Scientific™ MaxQ 4450 orbital shaker (Waltham, MA, USA) prewarmed to 37 °C at 120 rpm.

Chapter 5

Results and Discussion

5.1 Electrospun drug-eluting polylactic acid fibers

In this section, studies were performed to understand the physico-mechanical properties and in vitro drug release rates of electrospun drug-eluting polylactic acid (PLA) fibers to determine the effects of drug stabilities and drug loadings in hexafluoroisopropanol (HFIP) solvent during the solution preparation stage. Experimental results were reported from electrospun blank and drug-eluting PLA fibers using a small molecule model drug, acetylsalicylic acid (ASA).

5.1.1 Solution preparation and fiber electrospinning

The initial observation on the solution behavior of ASA in PLA-HFIP solution at 15% (w/w) loading suggested the miscibility of the drug and polymer in the organic solvent. After one day of mixing, no particles and/or residuals were observed in the blank PLA and PLA/ASA solutions, where polymer solutions became viscous enough that were ideal for electrospinning.

To investigate the effects of ASA stabilities in HFIP solvent during the solution preparation stage, ASA loaded PLA-HFIP solutions at 15% (w/w) were prepared after mixing for 1, 14, and 28 days. PLA/ASA solutions were visually examined for signs of drug degradation, such as residuals and changes in solution viscosity, color, and appearance. Qualitatively, there were no signs of ASA degradation in the PLA/ASA solution.

After electrospinning, disc samples of blank PLA and PLA/ASA fibers were prepared for imaging on their fiber morphologies and fiber mat microstructures using a scanning electron microscope (SEM). Representative SEM images are shown in Figure *5* for blank PLA and PLA/ASA fibers after mixing for 1, 14, and 28 days. According to the observations, PLA/ASA

fibers showed smooth fiber surfaces and uniform fiber mat structure without defects similar to those from the blank PLA fibers.

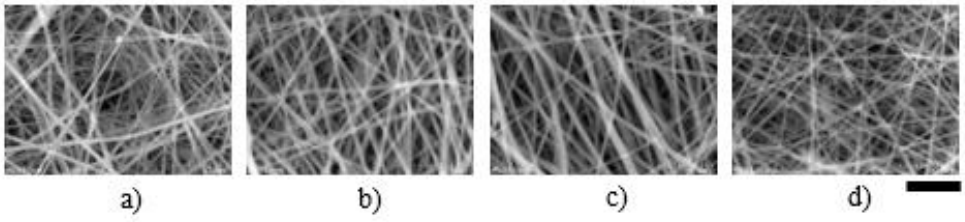

Figure 5. Scanning electron microscope images of electrospun PLA and PLA/ASA fibers on the effects of ASA stabilities in HFIP solvent, showing (a) blank PLA fibers (control groups), (b) PLA/ASA fibers (1 day), (c) PLA/ASA fibers (14 days), and (d) PLA/ASA fibers. Scale bar = 10μm.

After the successful initial trial of incorporating ASA in PLA-HFIP solutions at 15% (w/w) loading, loadings of ASA were increased to 30% and 45% (w/w) in the PLA-HFIP solutions. In particular, these solutions were prepared for 1 day only to test the solubility of ASA in the polymer system with a reasonable electrospinning time. After mixing, no particles and/or residuals were observed, suggesting the complete dissolution of the ASA in PLA-HFIP solutions up to 45% (w/w) loading. Increasing ASA loading increased the solution viscosity slightly; however, the PLA/ASA solutions were still in the manageable condition for electrospinning.

Disc samples of blank PLA and PLA/ASA fibers at various drug loadings (i.e., 15%, 30%, and 45% of ASA) were prepared for SEM imaging on their corresponding fiber morphologies and fiber mat microstructures. Representative SEM images are shown in Figure *6* for blank PLA and PLA/ASA fibers at various ASA loadings after 1 day of mixing. There were

no drug aggregates and drug recrystallizations on the surface of the fibers, indicating that the drugs were homogeneously encapsulated in the fibers up to 45% loading.

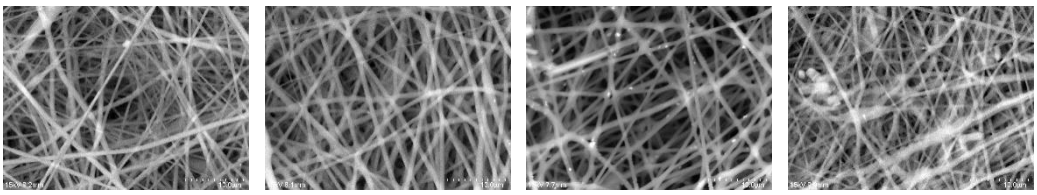

a) b) c) d)

Figure 6. Scanning electron microscope images of electrospun PLA and PLA/ASA fibers on the effects of ASA loadings, showing (a) blank PLA fibers (control groups), (b) PLA/ASA fibers (15%), (c) PLA/ASA fibers (30%), and (d) PLA/ASA fibers (45%). Scale bar = 10μm.

These experimental results suggested that PLA/ASA solutions prepared after 1, 14, and 28 days of mixing remained electrospinnable. Also, increasing drug loading up to 45%, followed by 1 day of mixing, showed no effects of drug aggregates on the fiber surfaces. In a similar study, electrospun PLA fibers were loaded with 14% (w/w) dexamethasone acetate (DEX) and 14% (w/w) betamethasone 17-valerate (BET) [107]. The fiber morphologies were homogenous with a bead-free surface, similar to our ASA-incorporated PLA fibers. Other studies reported the use of dichloromethane (DCM) solvent to introduce pores onto the fiber surfaces [108], where the porous microstructure on the fibers behaved as defects leading to a decrease in mechanical properties [109]. The porous fiber microstructure was not seen in our PLA/ASA fibers on mixing longevity and drug loading studies, indicating that HFIP solvent was compatible with PLA and ASA resulting in a porous-free and homogenous fiber structure.

5.1.2 Physico-mechanical properties and in vitro release behaviors of PLA/ASA fibers

5.1.2.1. Average fiber diameters

SEM images of blank PLA, PLA/ASA (1 day), PLA/ASA (14 days), and PLA/ASA (28 days) fibers were analyzed by the ImageJ software to obtain the average fiber diameter, and the results are shown in Figure *7*. The average fiber diameters for blank PLA, PLA/ASA (1 day), PLA/ASA (14 days), and PLA/ASA (28 days) groups were 0.69 ± 0.17 μm, 0.89 ± 0.16 μm, 0.74 ± 0.15 μm, and 0.63 ± 0.12 μm, respectively. Between the blank PLA and PLA/ASA (1 day) groups, the average fiber diameters were statistically different ($P < 0.05$). However, between the blank PLA and PLA/ASA (14 days) and PLA/ASA (28 days) groups, there were no statistical differences.

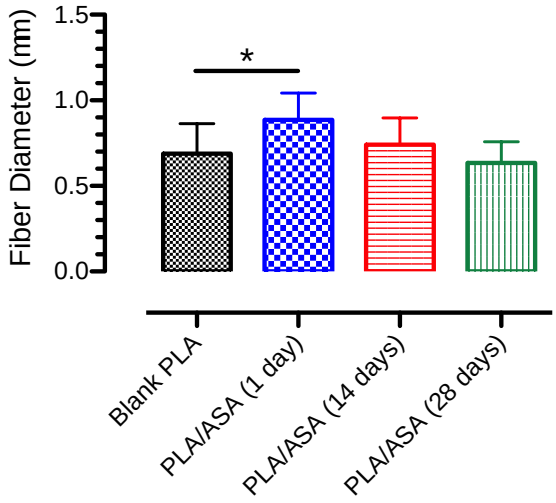

Figure 7. Average fiber diameters of electrospun blank PLA, PLA/ASA (1 day), PLA/ASA (14 days), and PLA/ASA (28 days) fibers (n = 30). An asterisk indicates statistical significance ($P < 0.05$).

SEM images from blank PLA and PLA/ASA fibers at various drug loadings (i.e., 15%, 30%, and 45% of ASA) were analyzed by the ImageJ software to obtain their average fiber diameters, and the results are shown in Figure *8*. The average fiber diameters for blank PLA, PLA/ASA (15%), PLA/ASA (30%) and PLA/ASA (45%) groups were 0.69 ± 0.17 μm, 0.89 ± 0.16 μm, 0.91 ± 0.19 μm, and 0.97 ± 0.28 μm, respectively. Between the blank PLA and the PLA/ASA (15%) groups, the average fiber diameters were statistically different ($P < 0.05$). However, there were no statistical differences within the PLA/ASA groups at various drug loadings.

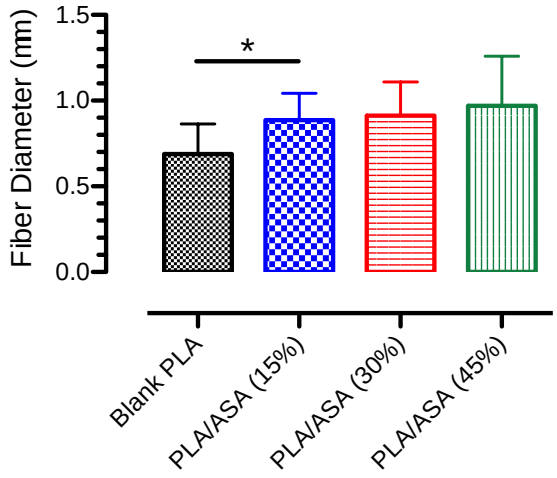

Figure 8. Average fiber diameters of electrospun blank PLA, PLA/ASA (15%), PLA/ASA (30%), and PLA/ASA (45%) fibers (n = 30). An asterisk indicates statistical significance ($P < 0.05$).

According to the data, the average fiber diameters of the electrospun PLA/ASA fibers were larger than the blank PLA fibers with and/or without statistical differences, likely due to the addition of drug as a solid component in the fibers. Specifically, the average fiber diameters of the PLA/ASA fibers showed a trend of decreasing after mixing for 28 days, suggesting the

potential dissociation of the drug crystals after prolonged exposure in the PLA-HFIP solution. In addition, increasing drug loading from 15% to 45% in the PLA fibers increased the average fiber diameters. This effect indicated that the addition of the drugs increased the overall solid contents in the solution for electrospinning, which produced fibers with larger average fiber diameters. Another aspect on the increases of the average fiber diameters were attributed to the intermolecular hydrogen-bonding and/or secondary non-covalent interactions of the drugs with the polymer molecule chains that increased the overall separation distances between the neighboring molecular chains [110].

5.1.2.2. Average fiber mat densities

Thickness and weight measurements of blank PLA, PLA/ASA (1 day), PLA/ASA (14 days), and PLA/ASA (28 days) fibers were taken and analyzed to determine the average fiber mat densities, and the results are shown in Figure *9*. The average fiber mat densities for blank PLA, PLA/ASA (1 day), PLA/ASA (14 days), and PLA/ASA (28 days) groups were 0.18 ± 0.01 g/cm^3, 0.31 ± 0.00 g/cm^3, 0.23 ± 0.01 g/cm^3, and 0.27 ± 0.01 g/cm^3, respectively. The differences between the control, PLA/ASA (1 day) and PLA/ASA (14 days) groups were statistically different ($P < 0.05$). However, there was no statistical difference between the PLA/ASA (14 days) and PLA/ASA (28 days) groups ($P > 0.05$).

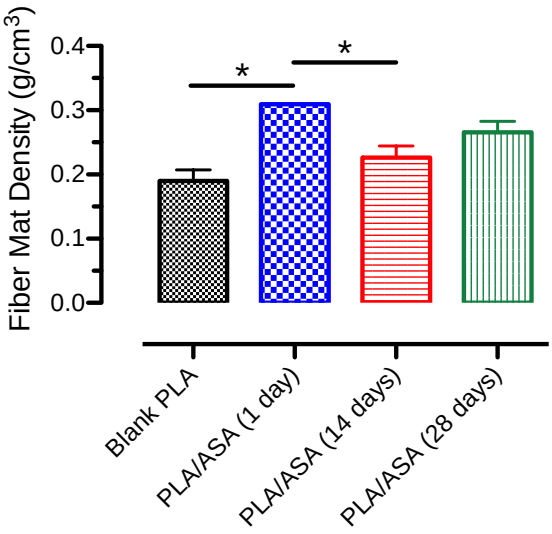

Figure 9. Average fiber mat densities of blank PLA, PLA/ASA (1 day), PLA/ASA (14 days), and PLA/ASA (28 days) fibers (n = 3). An asterisk indicates statistical significance ($P < 0.05$).

Thickness and weight measurements of blank PLA, PLA/ASA (15%), PLA/ASA (30%), and PLA/ASA (45%) fibers were taken and analyzed to determine the average fiber mat densities, and the results are shown in Figure *10*. The average fiber mat densities for blank PLA, PLA/ASA (15%), PLA/ASA (30%), and PLA/ASA (45%) groups were 0.18 ± 0.01 g/cm^3, 0.31 ± 0.00 g/cm^3, 0.33 ± 0.03 g/cm^3, and 0.31 ± 0.03 g/cm^3, respectively. The difference between the blank PLA and the PLA/ASA (15%) groups was statistically different ($P < 0.05$). However, there were no statistical differences among the PLA/ASA (15%), PLA/ASA (30%), and PLA/ASA (45%) groups ($P > 0.05$).

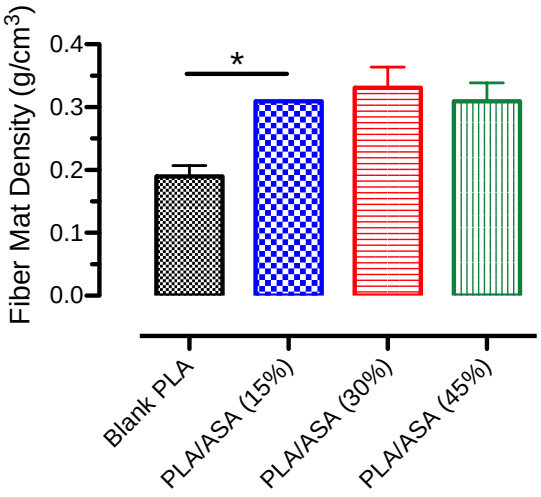

Figure 10. Average fiber mat densities of blank PLA, PLA/ASA (15%), PLA/ASA (30%), and PLA/ASA (45%) fibers (n = 3). An asterisk indicates statistical significance ($P < 0.05$).

According to the data, the average fiber mat densities increased with the addition of ASA in PLA fibers. Results also showed that the average fiber mat densities decreased slightly due to the increase of the mixing longevity. Studies suggested that the average fiber diameter played an important role in the average fiber mat densities [111]. Specifically, the trend in average fiber mat densities, as seen in Figure *9*, followed the results from the average fiber diameters for the ASA-loaded PLA fibers on the effects of mixing days, as seen in Figure *7*. In addition, similar trends were found in the PLA/ASA fibers with ASA loading up to 45%. The addition of 15% drugs increased the average fiber diameters and the fiber mat densities. However, as the drug loading increased to 45%, there was no further increase of average fiber diameter and fiber mat density. In a similar study, electrospun polyvinyl alcohol (PVA) fiber mats incorporated with sodium salicylate had a minimal difference in bead density as the amount of sodium salicylate increased [112].

5.1.2.3. Mechanical properties

A critical factor when considering a material for its potential use in drug delivery applications is the mechanical properties. Uniaxial tensile tests were performed on the electrospun blank PLA, PLA/ASA (1 day), PLA/ASA (14 days), and PLA/ASA (28 days) fibers. A representative stress strain curve can be seen in Figure *11*a. The stress strain curves after incorporation of ASA showed a necking behavior, which was associated with local plastic deformation of the PLA fibers.

Information regarding the elastic modulus can be observed in the initial viscoelastic region, which is the slope at the beginning of the stress strain curve. The average elastic modulus and average tensile strength are seen in Figure *11*b and Figure *11*c, respectively. The average elastic moduli were 82.65 ± 5.05 MPa, 138.64 ± 5.78 MPa, 124.71 ± 0.09 MPa, and 131.13 ± 0.25 MPa for the blank PLA, PLA/ASA (1 day), PLA/ASA (14 days), and PLA/ASA (28 days) groups, respectively. The ultimate tensile strengths were 2.74 ± 0.18 MPa, 4.92 ± 0.19 MPa, 3.52 ± 0.31 MPa, and 4.20 ± 0.32 MPa for the blank PLA, PLA/ASA (1 day), PLA/ASA (14 days), and PLA/ASA (28 days) groups, respectively. The increase in average elastic moduli and average tensile strengths indicated a strengthening effect due to the addition of the drug. This effect was the opposite of plasticizing in polymers that decreased the elastic modulus and ultimate tensile strength when incorporating a plasticizer in the polymer system [113]. This strengthening effect was reported in other studies when small amounts of drugs were added to a polymer [114–116].

The average elongation to failure is shown in Figure *11*d, and the values were 159.22 ± 5.27%, 181.74 ± 9.92%, 153.59 ± 2.28%, and 172.26 ± 6.82% for the blank PLA, PLA/ASA (1 day), PLA/ASA (14 days), and PLA/ASA (28 days) groups, respectively. The elongation to

failure slightly increased in the PLA/ASA (1 day) and PLA/ASA (28 days) groups as comparing to the control groups, suggesting an increase in fiber ductility from the addition of the drug.

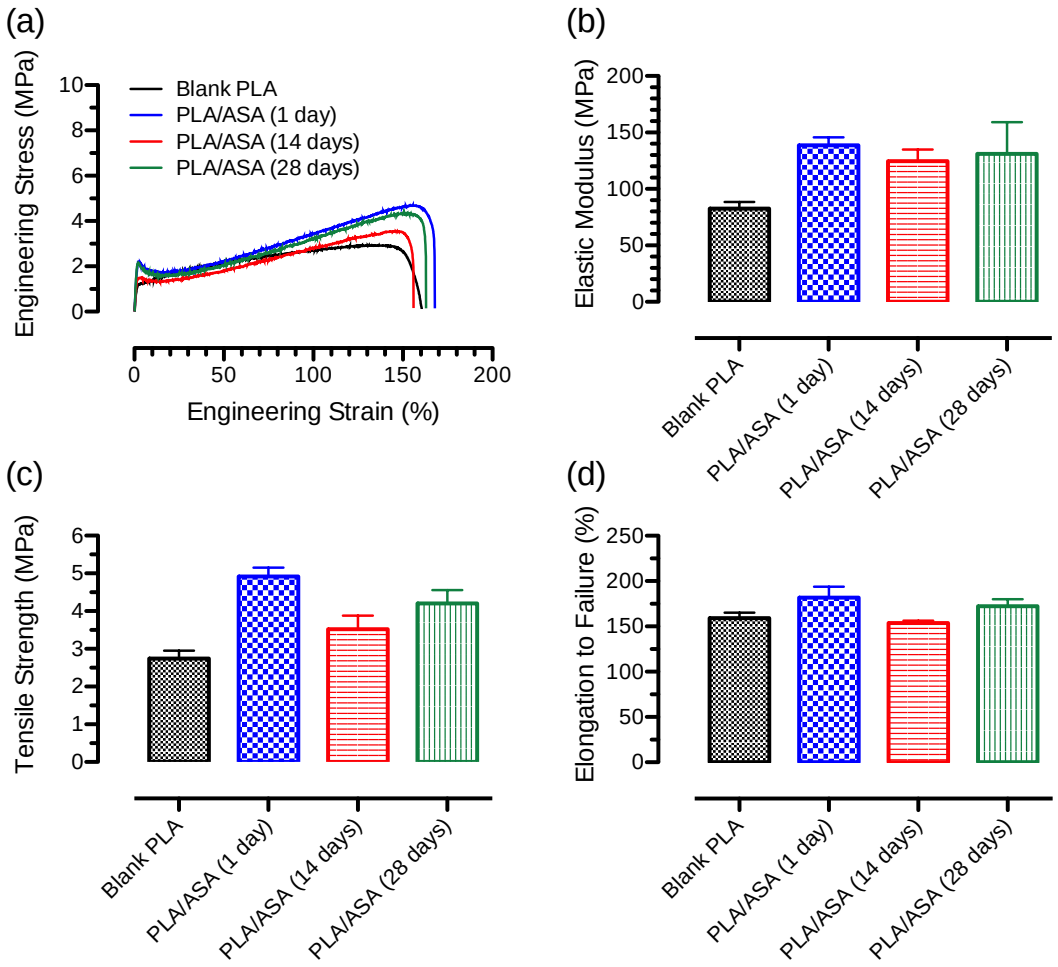

Figure 11. Tensile testing of blank PLA, PLA/ASA (1 day), PLA/ASA (14 days), and PLA/ASA (28 days) fibers, showing (a) representative stress strain curves, (b) average elastic moduli, (c) average tensile strengths, and (d) average elongation to failures (n = 4).

For the mechanical properties of blank PLA, PLA/ASA (15%), PLA/ASA (30%), and PLA/ASA (45%) fibers, representative stress strain curves are shown in Figure *12*a. The necking behaviors were visible from the stress strain curves of PLA/ASA (15%) and PLA/ASA (30%)

groups, where the PLA/ASA (45%) groups showed a slightly smaller necking behavior. This result indicated that the strengthening effect had reached a maximum level irrespective of the continuous increase in drug loading. When small molecules were incorporated into a semi-crystalline polymer (e.g., PLA) at a low concentration, favorable intermolecular interactions between the small molecules and the polymer matrix strengthened the amorphous region of the polymer resulting in a change in mechanical behavior leading to strengthening effects [117].

The average elastic moduli were 82.65 ± 5.05 MPa, 138.64 ± 5.78 MPa, 127.48 ± 8.59 MPa, and 97.42 ± 2.65 MPa for the blank PLA, PLA/ASA (15%), PLA/ASA (30%) and PLA/ASA (45%) groups, respectively, as seen in Figure *12*b. There was an increase from the blank PLA to the PLA/ASA (15%) groups followed by a slight decrease in the PLA/ASA (30%) and PLA/ASA (45%) groups. This slight decrease in the average elastic moduli due to drug loading showed that the strengthening effect had perhaps reached a saturation level in the amorphous regions of the PLA and that the further increase of the drug loading promoted minimal increase in the average elastic moduli. Similar effect was found in the average fiber diameter study, shown in Figure *7* and Figure *8*, associated with intermolecular couplings of the small molecule drugs and polymer matrix. In a similar study, cellulose acetate phthalate (CAP) films plasticized with tributyl citrate (TBC) were loaded with 64 μg of quercetin, and the elastic moduli of the films increased due to the strengthening effect [116]. However, the results showed a decrease of elastic moduli when the drug loading increased from 64 μg to 640 μg, indicating that a saturation level of the strengthening effect had been reached.

The ultimate tensile strengths were 2.74 ± 0.18 MPa, 4.92 ± 0.19 MPa, 3.64 ± 0.99 MPa, and 3.95 ± 0.57 MPa for the blank PLA, PLA/ASA (15%), PLA/ASA (30%) and PLA/ASA (45%) groups, respectively, as seen in Figure *12*c. The general trend of the average tensile

strengths decreased as drug loading increased for the PLA/ASA (15%) to the PLA/ASA (30%) and PLA/ASA (45%). The decrease in the average tensile strengths when increasing drug loading further supported the saturation of the strengthening effects in the PLA fibers, similar to the study performed using TBC films [118]. In general, the strengthening effect was the opposite of the plasticizing effect in polymer systems, where the ultimate tensile strength decreased due to the ease in molecular chain sliding and rupturing in the matrix.

The average elongation to failures were 159.22 ± 5.27%, 181.74 ± 9.92%, 124.42 ± 13.37%, and 144.18 ± 12.33% for the blank PLA, PLA/ASA (15%), PLA/ASA (30%) and PLA/ASA (45%) groups, respectively, as seen in Figure *12*d. The general trend of the average elongation to failure decreased when increasing ASA loading from 15% to 45%. The decrease in elongation to failure indicated a loss in the ductility of the fibers.

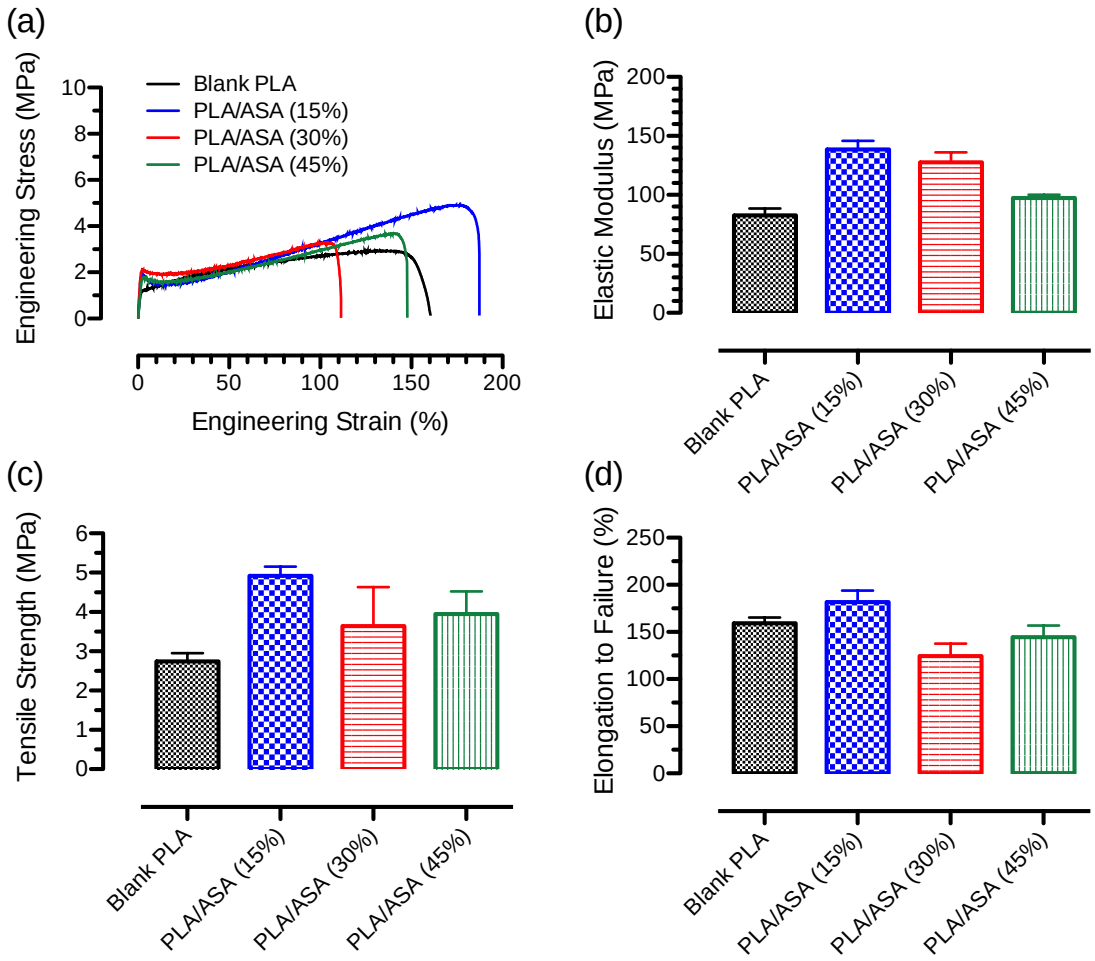

Figure 12. Tensile testing of blank PLA, PLA/ASA (15%), PLA/ASA (30%), and PLA/ASA (45%) fibers, showing (a) representative stress strain curves, (b) average elastic moduli, (c) average tensile strengths, and (d) average elongation to failures (n = 4).

5.1.2.4. In vitro drug release assays

Drug releases from biodegradable polymers is modulated through either diffusion of small molecule drugs or degradation of polymer matrix. The degradation process of a semi-crystalline polymer, such as PLA, occurs in two stages. The first stage starts with the infusion of water molecules into the amorphous region followed by the second stage that is characterized by the degradation of the amorphous region [119].

The average cumulative releases plateaued at around 60.93 ± 4.06%, 77.07 ± 4.70%, and 68.53 ± 7.38% for PLA/ASA (1 day), PLA/ASA (14 days), and PLA/ASA (28 days) groups, respectively, as seen in Figure *13*. The PLA/ASA (14 days) and PLA/ASA (28 days) groups showed a faster initial burst release than that of the PLA/ASA (1 day) group. The increasing drug release rate in PLA/ASA (14 days) and PLA/ASA (28 days) fiber groups supported the potential dissociation effects of the drug crystals in the polymer matrix as observed in Figure *7*.

Specifically, ASA broke down into smaller agglomerates due to the increased exposure in PLA-HFIP solution, which promotes free surface molecules that increased the release rate. Others reported the effects of smaller particles in drug release studies [120,121]. A non-linear curve fit analysis using one phase association showed that the rate constant, K values, were 0.15 ± 0.04, 0.66 ± 0.19, and 0.96 ± 0.54 for the blank PLA, PLA/ASA (1 day), PLA/ASA (14 days), and PLA/ASA (28 days) groups respectively. A larger K value indicated a faster release rate. The increasing K values showed that increasing mixing time in the solvent reduced the intermolecular bond strength between the PLA and the small molecule drugs allowing for a faster release rate.

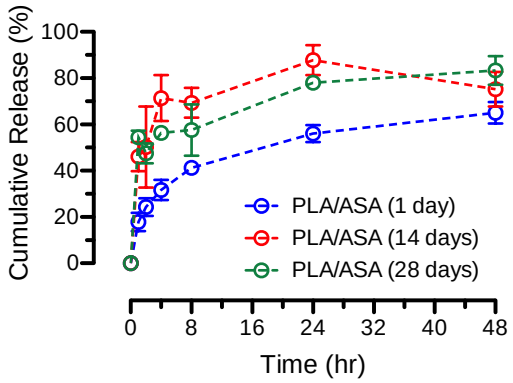

Figure 13. Cumulative drug release profiles of PLA/ASA (1 day), PLA/ASA (14 days), and PLA/ASA (28 days) fibers (n = 3).

For in vitro drug release assays using PLA/ASA fibers at various drug loadings, the average cumulative release rates plateaued at around 60.93 ± 4.06 %, 83.48 ± 3.49 %, and 89.42 ± 3.56 % for PLA/ASA (15%), PLA/ASA (30%) and PLA/ASA (45%) fiber groups, respectively, as seen in Figure *14*. The PLA/ASA (30%) and PLA/ASA (45%) groups had large initial burst release than the PLA/ASA (15%) groups. This indicated that more of the drug was released in the beginning time points, rather than a more controlled release as seen in the PLA/ASA (15%) groups. The increase in drug loading resulted in an increased amount of the free drugs in the fibers, which promoted the burst release behavior. Similar results were seen by other researchers with drug-loaded fibers [122,123]. A non-linear curve fit analysis using one phase association showed that the rate constant, K values, were 0.15 ± 0.04, 0.41 ± 0.07, and 0.21 ± 0.03 for PLA/ASA (15%), PLA/ASA (30%) and PLA/ASA (45%) fiber groups, respectively. These K values were smaller than those after 14 and/or 28 days of mixing in the solvents, suggesting that the role of drug dissociation is more important than drug loading in fibers. These in vitro drug release assays demonstrated the effects drug-polymer interactions in the polymer matrix for controlled release behaviors of small molecule drugs.

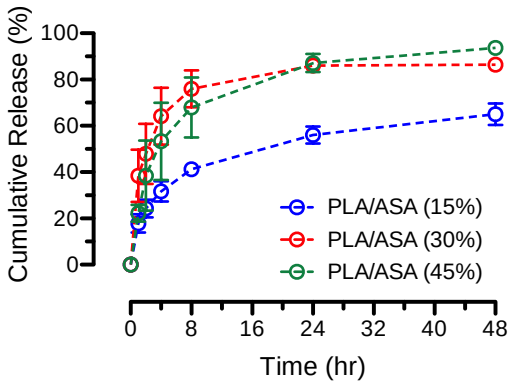

Figure 14. Cumulative drug release profiles of PLA/ASA (15%), PLA/ASA (30%), and PLA/ASA (45%) fibers (n = 3).

5.1.2.5. Fiber mechanical properties after drug releases

The ability to maintain fiber mechanical properties after drug release is a critical factor for the design of electrospun drug-eluting fibers in biomedical applications. Representative stress strain curves of blank PLA after 2 and 48 hours of incubation in the release media, denoted as control, 2 hrs, and 48 hrs groups, respectively, are shown in Figure *15*a. There was no change to the necking behavior in stress strain curves for all samples since there was no addition of drug in the fibers.

The average elastic moduli of the blank PLA fibers were 101.50 ± 12.98 MPa, 68.90 ± 24.74 MPa, and 96.16 ± 16.32 MPa for the control, 2 hrs, and 48 hrs groups, respectively, as seen in Figure *15*b. There was no statistical difference between each of the groups ($P > 0.05$). This indicated that the stiffness of PLA fibers was unaffected after incubation in the PBS for up to 48 hrs. The average tensile strengths of the blank PLA fibers were 3.86 ± 0.29 MPa, 4.19 ± 0.1 MPa, and 4.30 ± 0.37 MPa for the control, 2 hrs, and 48 hrs groups, respectively, as seen in Figure *15*c. The minimal changes in the average elastic moduli and the average tensile strengths

indicated that the release media had little effect in degrading the PLA polymer over the course of study. In a similar study, the tensile strength of PLLA fibers showed almost no changes during the in vitro degradation assays in PBS at 80°C [124]. The average elongations to failure of the blank PLA fibers were 124.38 ± 3.71%, 147.87 ± 25.35%, and 123.28 ± 10.84% for the control, 2 hrs, and 48 hrs groups, respectively, as seen in Figure *15*d. There were no statistical differences between the groups, indicating again that the release media had little effect on the degradation of the PLA polymer matrix.

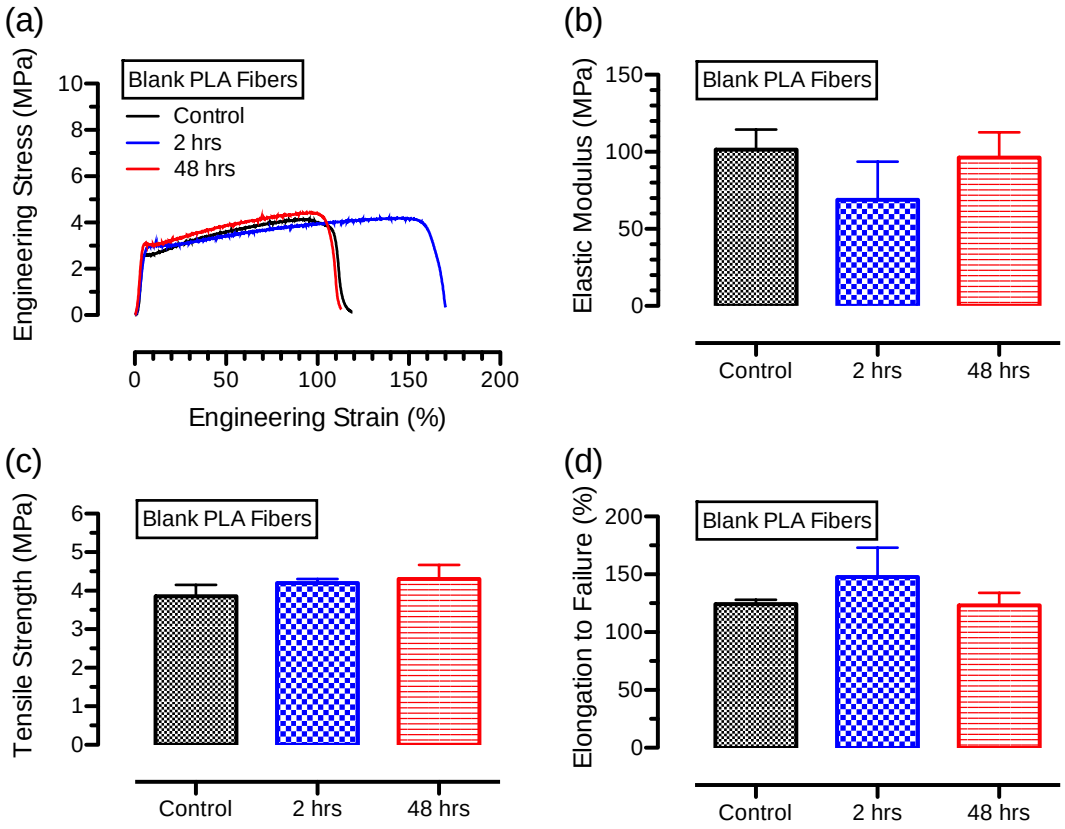

Figure 15. Mechanical properties of blank PLA fibers after degradation assays, showing (a) representative stress strain curves, (b) average elastic moduli, (c) average tensile strengths, and (d) average elongation to failures for control, 2 hrs, and 48 hrs groups (n = 4).

In comparison to the mechanical properties of blank PLA fibers after degradation in the PBS release media, the mechanical properties of PLA/ASA drug-eluting fibers after in vitro drug release assays were studied using the PLA/ASA groups using 15% ASA loading for 1 day mixing of the ASA in PLA-HFIP. The representative stress strain curves are shown in Figure *16*a for the PLA/ASA control fibers, PLA/ASA fibers after 2 hours of drug release, and PLA/ASA fibers after 48 hours of drug release. These fibers were denoted as control, 2 hrs, and 48 hrs groups, respectively.

The necking behavior disappeared when increasing the drug release time in the release media. This effect indicated that the mechanical properties were affected as the small molecule drugs diffused out from the PLA matrix, which loosened the intermolecular bonding between the PLA molecular chains.

The average elastic moduli for the PLA/ASA fibers were 138.64 ± 7.08 MPa, 54.11 ± 15.19 MPa, and 72.24 ± 16.58 MPa for the control, 2 hrs, and 48 hrs groups, respectively, as shown in Figure *16*b. There was a significance difference ($P < 0.05$) between the control groups and the 2hrs groups. However, there was no significance difference between the 2 hrs groups and the 48 hrs groups ($P > 0.05$).

The ultimate tensile strengths for the PLA/ASA fibers were 4.92 ± 0.24 MPa, 3.55 ± 0.54 MPa, and 5.65 ± 1.09 MPa for the control, 2 hrs, and 48 hrs groups, respectively, as shown in Figure *16*c. There was a significant difference between the control groups and the 2 hrs groups ($P < 0.05$). Along with the findings from the average elastic moduli, this result demonstrated the decrease of mechanical properties as the drugs diffused out from the PLA matrix. It has been found in similar studies that over time the elastic modulus and tensile strength of polyester fibers decreased after drug release [125].

The average elongation to failure for the PLA/ASA fibers were 181.63 ± 12.15%, 121.10 ± 46.04%, and 84.72 ± 13.66% for the control, 2 hrs, and 48hrs groups, respectively, as shown in Figure *16*d. There were significant decreases in the average elongation to failures for the drug release groups (i.e., 2 hrs and 48 hrs groups) as compared to the control groups ($P < 0.05$). This decrease indicated the loss of the intermolecular bonding of the PLA matrix.

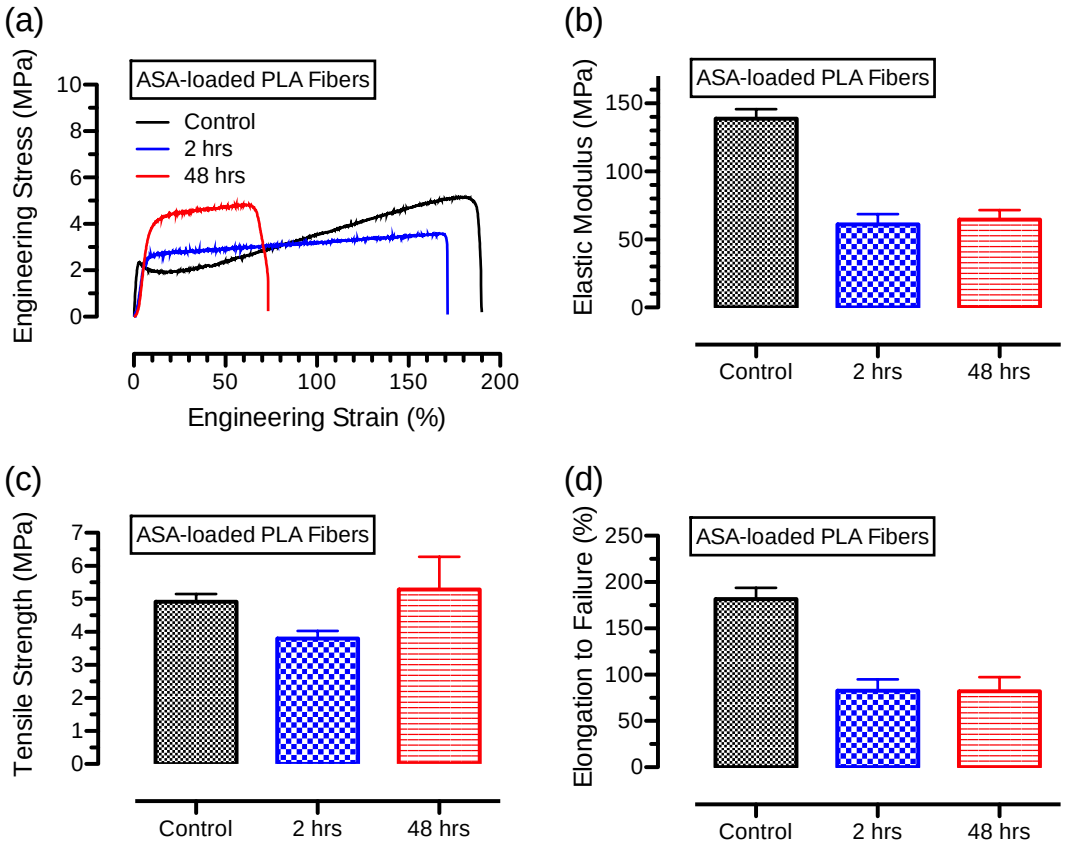

Figure 16. Mechanical properties of ASA-loaded PLA fibers after drug release assays, showing (a) representative stress strain curves, (b) average elastic moduli, (c) average tensile strengths, and (d) average elongation to failures for control, 2 hrs, and 48 hrs groups (n = 4).

5.2. Hydrogen peroxide vapor calibration studies

Prior to the materials compatibility studies on the effects of hydrogen peroxide vapor on electrospun drug-eluting PLA fibers, a series of tests were performed to validate the ability of the portable device to generate hydrogen peroxide vapor. The initial pilot studies included hydrogen peroxide vapor calibration runs using various concentrations of liquid hydrogen peroxide to determine the steady state conditions inside an enclosed glove box. In addition, hydrogen peroxide vapor generated from 35% concentration of liquid hydrogen peroxide was used to determine various levels of concentration-time exposure for the electrospun drug-eluting PLA fibers.

5.2.1 Effects of liquid hydrogen peroxide concentrations

The correlations of hydrogen peroxide vapor concentration in an enclosure with the use of various concentrations of liquid hydrogen peroxide as the source enabled the determination of steady-state conditions. A steady-state condition on the hydrogen peroxide vapor concentration was accompanied with the stabilization of the relative humidity and the temperature within the enclosure. To evaluate the effects of various concentrations of liquid hydrogen peroxide on the steady-state conditions, four concentrations of liquid hydrogen peroxide of 3.5%, 10%, 20%, and 30% (v/v) were chosen. This initial experiment allowed us to observe if a stock 35% liquid hydrogen peroxide, which was widely employed in the Steris® VHP systems, may be used as the source in our portable device to generate hydrogen peroxide vapor at the appropriate level.

Both the relative humidity and temperature inside the glove box played important roles in the saturation level of hydrogen peroxide vapor concentration when reaching a steady-state condition. Figure *17* illustrated the effects of relative humitidies and temperatures within an enclosed glove box on hydrogen peroxide liquids with concentrations of 3.5%, 10%, 20%, and

30%, respectively. The relative humidity quickly increased for all the groups and then started to plateau after 30 minutes into the process. The relativity humidity plateaued in between 80% and 88% for various concentrations of liquid hydrogen peroxide over 200 minutes ireespective of the initial starting relative humidity. The outdoor relative humidity was taken also, but it was determined it had no effect on the indoors relative humidity. In addition, the temperatures fluctuated slightly at the beginning of the experiment for all four groups of the corresponding liquid hydrogen peroxides. The temperature experienced a drop due to a evaporative cooling effect cause by the fan on the device. However, all four groups reached an equilibrium at 21°C within 60 minutes. These observations indicated that the temperature and relative humidity were able to reach a steady-state condition using various liquid hydrogen peroxide as the source. Moreover, this study also provided preliminary information on the experiemntal safety when using highly concentrated hydrogen peroxide liquid to generate hydrogen peroxide vapor.

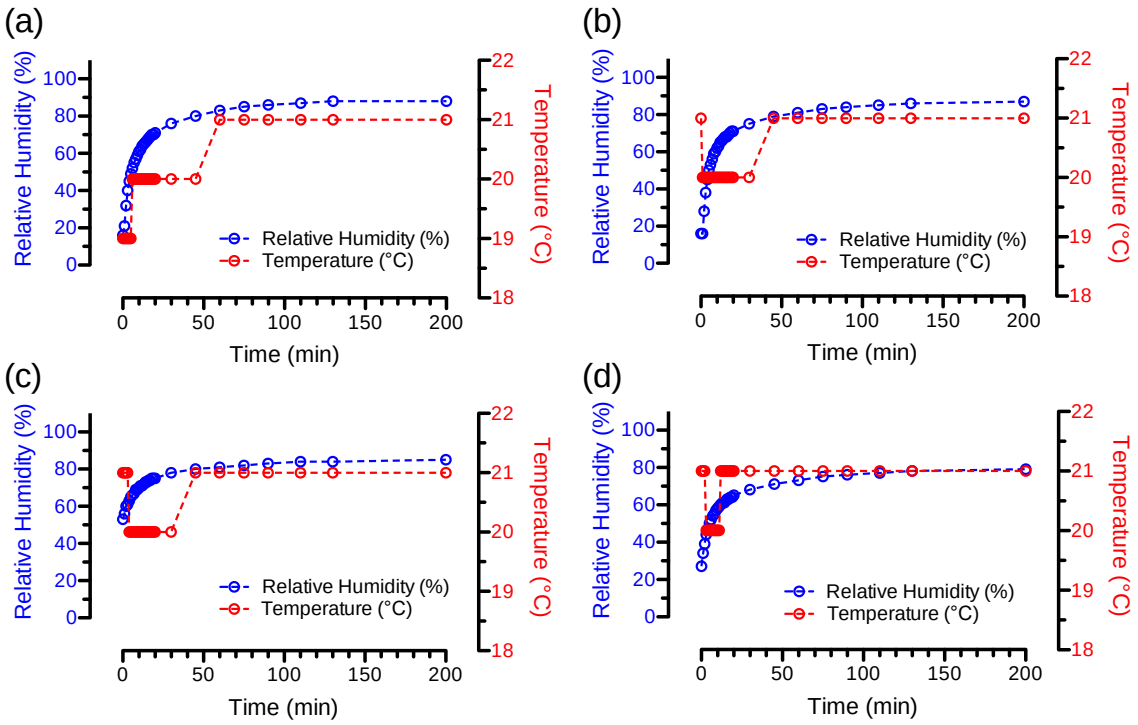

Figure 17. The effects of relative humidity (%) and Temperature (°C) on (a) 3.5%, (b) 10%, (c) 20%, and (d) 30% liquid hydrogen peroxide over 200 minutes inside the glove box.

In order to achieve a 6-log kill for bateria and viruses, the concentration of the hydrogen peroxide vapor is typically 180-200 ppm within an enclosure. In our initial test run, the concentration of hydrogen peroxide vapor gradually increased and reached a plateau at around 10 – 15 ppm after 40 minutes when using the 3.5% and 10% liquid hydrogen peroxide as the source. The concentration of hydrogen peroxide vapor plateaued at around 60 ppm after 60 minutes and at around 100 ppm after 90 minutes when using the 20% and 30% liquid hydrogen peroxide as the souce, respectively, as seen in Figure *18*. The plateau of the hydrogen peroxide vapor concentration increased with the increase of the liquid hydrogen peroxide concentration as the source. This finding was expected as the 30% group had a higher hydrogen peroxide partial

pressure in the enclosure when reaching equilibrium. Since water and hydrogen peroxide have a very similar molecular structure, hydrogen peroxide also affects the relative humidity [126]. Since the temperature remained constant throughout the experiments, the saturated vapor pressure was the same. As the hydrogen peroxide partial pressure increased, the water partial pressure decreased [127], which allowed for the total partial pressure to stay constant. Thus, the relative humidity plateaued at approximately the similar point for all the concentrations.

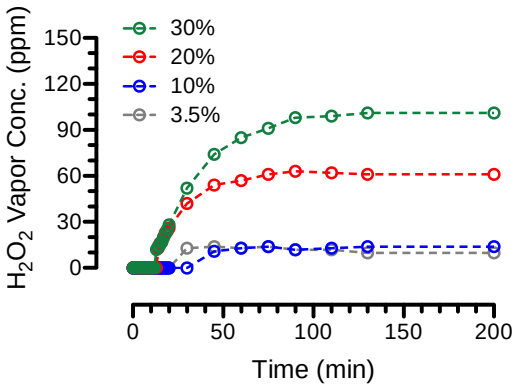

Figure 18. Hydrogen peroxide vapor concentration profiles using 3.5%, 10%, 20%, and 30% of liquid hydrogen peroxide as the source for over 200 minutes inside a glove box.

To compare the effects of the rate constants on the increase of relative humidity regardless of the starting humidity for each groups, the raw data was normalized. The normalized relativity humidities plateaued at 0.95, 0.93, 0.93, and 0.92 for the 3.5%, 10%, 20%, and 30% liquid hydrogen peroxide, respectively, as seen in Figure *19*. The plateaus of the normalized data indicated, that regardless of the starting relative humidity and the concentration of the liquid hydrogen peroxide as the source, the final relative humidity acheived a steady-state at approximately 90% of the capacity. The rate constant were 0.095 min^{-1}, 0.115 min^{-1}, 0.072 min^{-1}, and 0.086 min^{-1} for the 3.5%, 10%, 20%, and 30% groups, respectively. These rate constants also

suggested that the relative humidity increased at approximately the same rate regardless of the starting concentration of the liquid hydrogen peroxide.

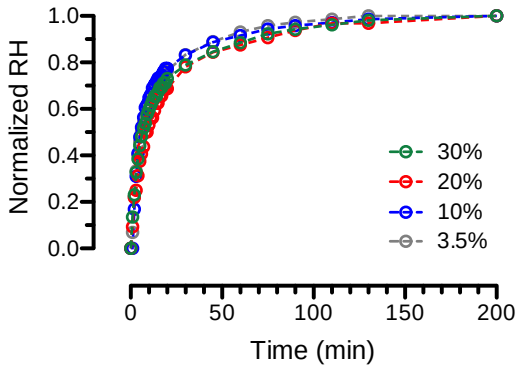

Figure 19. Normalized relative humidity profiles using 3.5%, 10%, 20%, and 30% liquid hydrogen peroxide as the source for over 200 minutes inside the glove box.

5.2.2 35% liquid hydrogen peroxide

After confirming the effects of various concentrations of liquid hydrogen peroxide on the steady-state conditions within the enclosure, attempts were made to determine the three effective hydrogen peroxide vapor time-concentration levels using 35% hydrogen peroxide as the source. A concentration of 35% liquid hydrogen peroxide was choosen since it was used as the source to produce hydrogen peroxide vapor in the Steris® systems [14]. Representative curves of the relative humidity and hydrogen peroxide vapor concentration using the 35% liquid hydrogen peroxide as the source are shown in Figure *20*. It can be seen that the relative humidity and hydrogen peroxide vapor concentration quickly increased for approximately the first 30 minutes and then started to level out at approximately 80-90% and 180-200 ppm for the relative humidity and hydrogen peroxide vapor concentration, respectively.

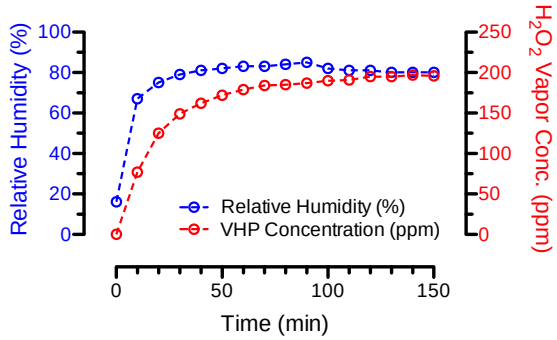

Figure 20. Representative hydrogen peroxide vapor concentration and relative humidity profiles using 35% liquid hydrogen peroxide as the source for over 150 minutes inside the glove box.

Using the 35% liquid hydrogen peroxide as the source, the hydrogen peroxide vapor concentration generated from the portable device within the glove box was determined to be comparable with typical commercial vapor phase hydrogen peroxide decontamination units, which were capable of generating hydrogen peroxide vapor concentration in the range of 150-600 ppm [128]. For this work, three hydrogen peroxide vapor concentration-time levels were chosen to evaluate the effects of vapor phase hydrogen peroxide on materials properties of the electrospun blank and ASA-loaded PLA fibers. To determine the three effective hydrogen peroxide vapor time-concentration levels for the study, values on the relative humidity, temperature, and hydrogen peroxide vapor concentration were taken every 15 minutes. Once the relative humidity and the hydrogen peroxide vapor concentration were stabilized, fibers were exposed to hydrogen peroxide vapor for 1, 3, and 5 hour. The area under the hydrogen peroxide concentration curve was calculated to be 10,800 ppm-min, 37,000 ppm-min, and 58,000 ppm-min each of the vapor hydrogen peroxide exposure levels referred to low, medium and, high effective concentration-time of vapor hydrogen peroxide cycles, respectively. These levels were

choosen as they correlated to approximate time-concentration levels of a typical commercialized vapor phase hydrogen peroxide unit.

5.3. Decontamination of Polylactic Acid Fibers

In this section, electrospun blank polylactic acid (PLA) fibers as well as fibers incorporated with acetylsalicylic acid (ASA) as a model drug, 15% (w/w) loading and mixing for 1 day, were subjected to low, medium, and high level of hydrogen peroxide vapor treatments to determine the materials compatibility of the fibers. Physico-mechanical studies were performed, including fiber morphologies and average fiber diameters, fiber mat physical properties, and mechanical properties, to correlate with the chemical analysis and the in vitro drug release behaviors of the PLA/ASA fibers to determine the effects of the hydrogen peroxide vapor treatments on the drug-eluting fibers.

5.3.1. Fiber morphologies and fiber mat microstructures

Analysis of the fiber morphologies allows for the observations of surface degradation and/or oxidation due to chemical-related damage on the electrospun fibers after hydrogen peroxide vapor treatments. Disc samples of blank PLA fibers without hydrogen peroxide treatment (i.e., control) and those treated with hydrogen peroxide vapor at various levels (i.e., low, medium, and high) were prepared for SEM imaging on their corresponding fiber morphologies and fiber mat microstructures.

Representative SEM images of the blank PLA fibers with and without hydrogen peroxide vapor treatments are shown in Figure *21*. According to the observations, the blank PLA fibers treated with various levels of hydrogen peroxide vapor exposure showed smooth fiber surface and uniform fiber mat structure without defects similar to the blank PLA control groups. This observation indicated no degradation and oxidation occurred on the fiber surfaces after hydrogen

peroxide vapor treatments. Similar results were seen on the surface morphologies of polyester fibers [129].

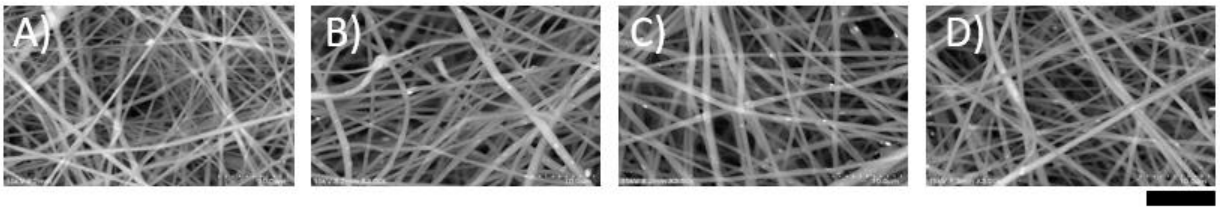

Figure 21. SEM images of electrospun blank PLA fibers, showing (a) control fibers, (b) fibers after low level, (c) medium level, (d) high level of hydrogen peroxide vapor treatments using 35% liquid hydrogen peroxide as the source. Scale bar = 10 μm.

Disc samples of ASA-loaded PLA fibers without hydrogen peroxide treatment (i.e., control) and those treated with various levels of hydrogen peroxide vapor (i.e., low, medium, and high) were prepared for SEM imagining on their corresponding fiber morphologies and fiber mat microstructures. Representative SEM images of the ASA-loaded PLA fibers with and without hydrogen peroxide vapor treatments are shown in Figure *22*. Microscopic evaluations suggested smooth and defect-free fibers with no drug aggregates on the surface of the fibers. This observation indicated the compatibility of hydrogen peroxide vapor after various levels of treatments on the physical shapes of the drug-eluting fibers.

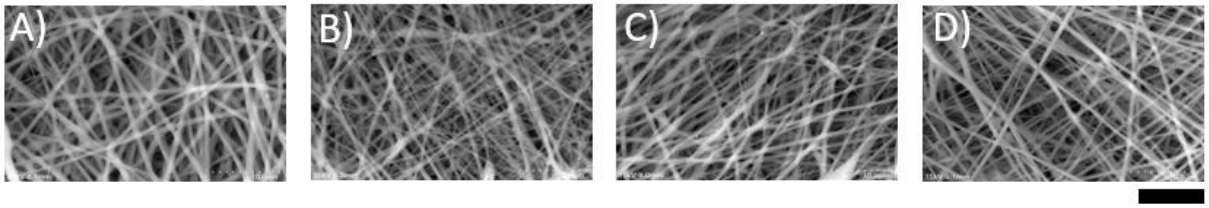

Figure 22. SEM images of electrospun ASA-loaded PLA fibers, showing (a) control fibers, (b) fibers after low level, (c) medium level, (d) high level of hydrogen peroxide vapor treatments using 35% liquid hydrogen peroxide as the source. Scale bar = 10 μm.

5.3.2. Average fiber diameters

Analysis of the fiber diameter allows for the quantitative understanding on the effects of hydrogen peroxide vapor treatments on the electrospun blank and ASA-loaded PLA fibers. SEM images from the blank PLA fibers without hydrogen peroxide treatment (i.e., control) and those treated with various levels of hydrogen peroxide vapor (i.e., low, medium, and high) were analyzed by the ImageJ software to obtain the average fiber diameters, and the results are shown in Figure *23*. The average fiber diameters showed no statistically difference ($P > 0.05$) at 0.82 ± 0.12 μm, 0.85 ± 0.14 μm, 0.83 ± 0.12 μm, and 0.87 ± 0.15 μm for blank PLA fibers of control, low, medium, and high groups, respectively.

SEM images of ASA-loaded PLA fibers without hydrogen peroxide treatment (i.e., control) and those treated with various levels of hydrogen peroxide vapor (i.e., low, medium, and high) were analyzed by the ImageJ software to obtain the average fiber diameter, and the results are shown in Figure *23*. The average fiber diameter for ASA-loaded PLA fibers of control, low, medium, and high groups were 0.81 ± 0.14 μm, 0.70 ± 0.11 μm, 0.72 ± 0.17 μm, and 0.74 ± 0.10 μm, respectively. Between the control and the low groups of ASA-loaded PLA fibers, there was

a statistical difference on the average fiber diameters ($P < 0.05$). However, between the various concentration-time exposure levels, there were no statistical differences on the average fiber diameters ($P > 0.05$).

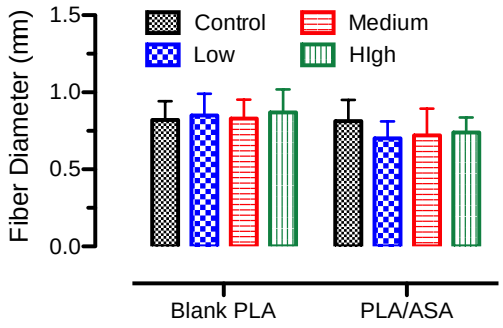

Figure 23. Average fiber diameter of the blank PLA and ASA-loaded fibers after various levels of hydrogen peroxide vapor treatments using 35% liquid hydrogen peroxide as the source.

According to the data, the average fiber diameters showed no changes after various levels of the hydrogen peroxide vapor concentration-time exposures on the blank PLA fibers. This indicated that the hydrogen peroxide vapor had minimal degradation and/or oxidation effects on the PLA fibers. However, with the ASA-loaded PLA fibers, the average fiber diameters decreased significantly after subjecting to various levels of hydrogen peroxide vapor concentration-time exposure as compared to the control groups. This decrease indicated that some levels of interactions between the hydrogen peroxide vapor and its by-product of water molecules with the ASA encapsulated inside the fibers. This interactions was likely to interrupt the hydrogen bonds between the drug molecules and the PLA molecular chain [110]. There was no continuous decrease in average fiber diameter as the levels of hydrogen peroxide vapor concentration-time exposure increased, indicating perhaps the bond interruptions had reached a saturation level after the low level exposure.

5.3.3. Physical Properties

A major concern with the use of hydrogen peroxide vapor as a decontamination choice is with its materials compatibility, especially for polymers that tend to absorb hydrogen peroxide vapor into the materials causing degradation and oxidation effects. Since the purpose of the drug-eluting fibers is to be used in biomedical applications, there is a concern that hydrogen peroxide vapor could damage the fibers during the hydrogen peroxide vapor exposure process. In this regard, analyses of the area and weight change allow for the evaluation of potential degradation in the physical properties of the fibers due to the absorption of the hydrogen peroxide vapor.

Circular fiber discs of ½" in diameter were used to examine the area change evaluated by ImageJ software before and after various levels of hydrogen peroxide vapor concentration-time exposures. The average percentage area changes for the blank PLA fibers were 0.70 ± 1.92%, 1.26 ± 0.54% and 3.10 ± 1.00% for the low, medium, and high groups, respectively, as seen in Figure *24*. The average percentage area changes for the ASA-loaded PLA fibers were 0.40 ± 1.05%, 0.18 ± 0.26% and -0.54 ± 0.33% for the low, medium, and high groups, respectively, as seen in Figure *24*.

The blank PLA fibers had a minimal change in the area as the exposure level of concentration-time increased. This indicated that the hydrogen peroxide vapor did not deform the samples through shrinkage or swelling effects. However, the ASA-loaded PLA fibers experienced a decrease in area as the exposure levels of concentration-time increased. A similar study found that the percentage area decreased due to the increase in hydrolysis time [130]. This finding indicated that the addition of the ASA in the PLA fibers caused an increase level in the hydrolysis degradation of the PLA.

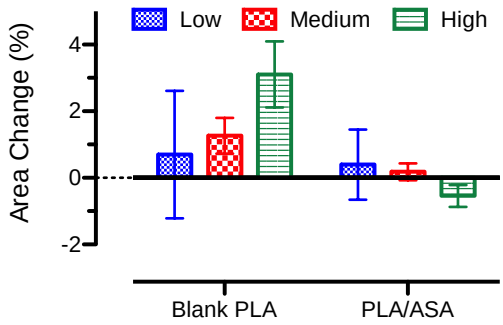

Figure 24. Percentage area change of the blank PLA and ASA-loaded PLA fibers after various levels of hydrogen peroxide vapor treatments using 35% liquid hydrogen peroxide as the source.

Circular fiber discs of ½" in diameter were weighed before and after various levels of hydrogen peroxide vapor concentration-time exposures. The average percentage weight changes of the blank PLA fibers were 4.55 ± 5.25%, 1.92 ± 3.85%, and 0.63 ± 4.48% for the low, medium, and high groups, respectively, as seen in Figure *25*. The average percentage weight changes of the ASA-loaded PLA fibers were 0.79 ± 4.42%, -3.87 ± 10.56%, and -4.96 ± 9.11% for the low, medium, and high groups, respectively, as seen in Figure *25*.

The blank PLA fibers had a minimal change in weight as the levels of hydrogen peroxide vapor concentration-time exposure increased. This result indicated that the blank fibers were not absorbing the moisture irrespective of the levels of hydrogen peroxide vapor concentration-time exposures since PLA is one of the hydrophobic polyesters. The drug-loaded fibers exhibited a decrease in weight changes as the levels of hydrogen peroxide vapor concentration-time exposure increased. ASA consists of carboxyl groups (-COOH) [131], which is a hydrophilic functional group. In other words, the addition of the ASA to the polymer attracts moisture during the decontamination process. The decrease in weight of the ASA-loaded PLA fibers indicates

that there was some interactions between the hydrogen peroxide vapor with ASA that led to the degradation of the small molecule drugs resulting in the loss of overall fiber mass.

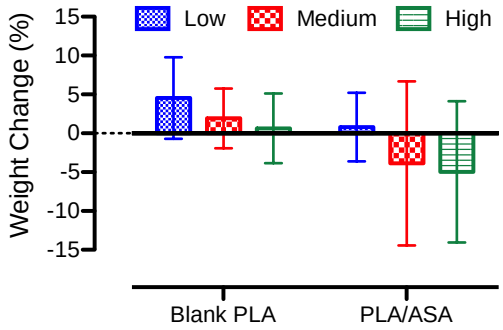

Figure 25. Percentage weight change of the blank PLA and ASA-loaded PLA fibers after various levels of hydrogen peroxide vapor treatments using 35% liquid hydrogen peroxide as the source.

5.3.4. Mechanical Properties

A critical factor when considering a material for the potential use in drug delivery applications is the mechanical properties. When introducing a drug delivery device to the human body, the device has to have the ability to perform under various kinematic conditions. A concern was that after vapor phase hydrogen peroxide treatment, the material would become too brittle to be used in drug delivery applications.

The mechanical properties of the drug-eluting fibers after vapor phase hydrogen peroxide treatments were determined using tensile testing. Three samples were taken from the blank PLA and PLA/ASA fibers after exposing to various levels of the low, medium, and high time-concentration treatments. These samples underwent a constant strain rate until the samples fractured. The stress strain curves were plotted to determine the average Young's moduli, average tensile strength, and average elongation to failure.

An initial viscoelastic region can be seen on the stress-strain curve where the stress increased rapidly with a minimal increase of strain. After the linear viscoelastic region, stress increased minimally with an increasing of strain as seen in Figure *26*a for the blank-PLA.

Information regarding the average elastic moduli can be observed from the initial viscoelastic region, which is the slope at the beginning of the curve. The average moduli for the blank PLA fibers were 83.4 ± 3.8 MPa, 84.2 ± 8.2 MPa, 86.2 ± 6.9 MPa, and 85.7 ± 16.1 MPa for the control, low, medium, and high groups, respectively, as seen in Figure *26*b.

The last region of the stress-strain curve is associated with the strain-hardening effect, and this is quantified by the tensile strength of the material, which is found at the peak of the curve, the point at which the material fails. The average tensile strength of the blank PLA fibers is shown in Figure *26*c, and they are 2.74 ± 0.21 MPa, 3.39 ± 0.23 MPa, 3.53 ± 0.24 MPa, and 3.60 ± 0.68 MPa for the control, low, medium, and high groups, respectively.

Lastly, the elongation to failure corresponds to the overall percentage of deformation that was applied to the fibers before failure occurred. The average elongation to failure of the blank PLA fibers is shown in Figure *26*d, and they are 159.2 ± 6.1%, 126.0 ± 13.9%, 137.8 ± 13.4%, and 127.0 ± 11.6% for the control, low, medium, and high groups, respectively.

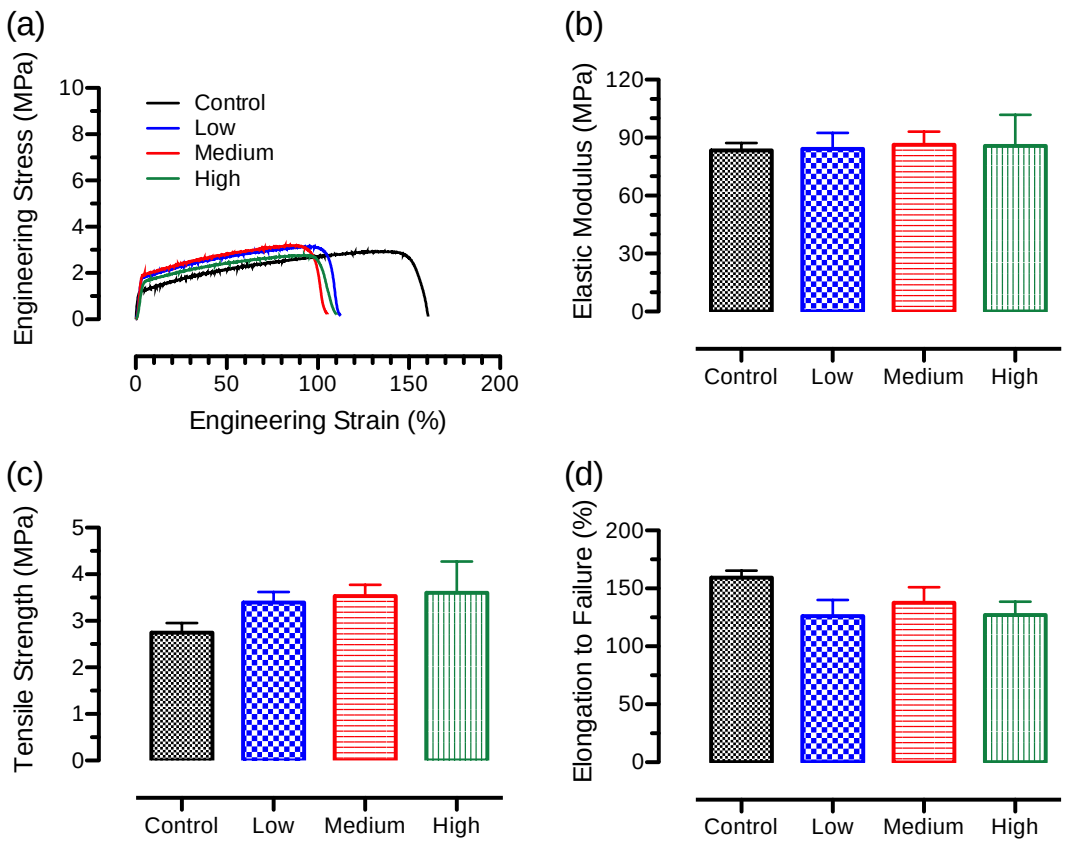

Figure 26. Mechanical properties for blank PLA fibers, showing (a) representative stress strain curves, (b) average elastic moduli, (c) average tensile strength, and (d) average elongation to failure of the control, low, medium, and high level of hydrogen peroxide vapor treatment using 35% liquid hydrogen peroxide as the source.

A representative stress strain curve for the ASA-loading PLA fibers after various levels of vapor phase hydrogen peroxide treatments can be seen in Figure *27*a. The average moduli for PLA/ASA fibers were 138.63 ± 7.07 MPa, 119.27 ± 0.33 MPa, 65.46 ± 17.28 MPa and 73.68 ± 21.58 MPa for control, low, medium, and high groups, respectively, as seen in Figure *27*b. The average tensile strength of the PLA/ASA fibers is found in Figure *27*c, and they are 4.92 ± 0.23 MPa, 4.82 ± 0.63 MPa, 3.62 ± 0.88 MPa, and 4.21 ± 0.36 MPa for control, low, medium, and

high groups, respectively. The average elongation to failure of the PLA/ASA fibers investigated is found in Figure *27*d, and they are 181.64 ± 12.15%, 138.41 ± 43.97%, 128.39 ± 5.48%, and 117.69 ± 24.25% for control, low, medium, and high groups, respectively.

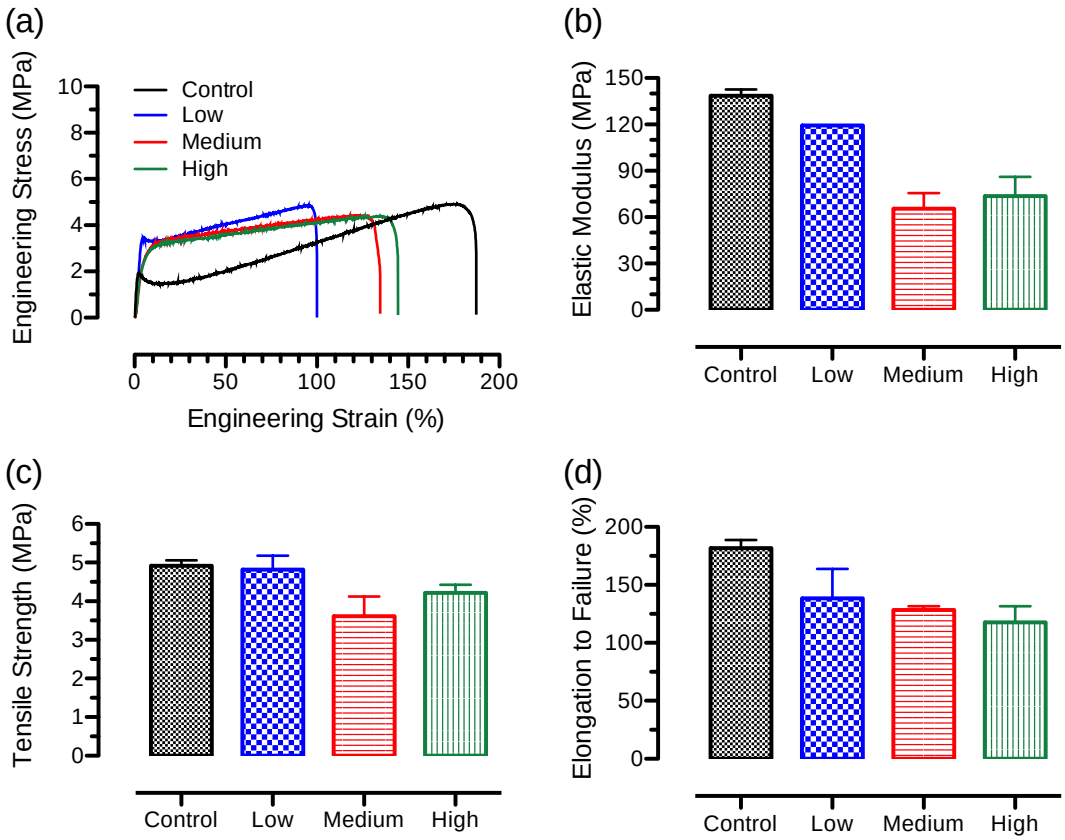

Figure 27. Mechanical properties for ASA-loaded PLA fibers, showing (a) representative stress strain curves, (b) average elastic moduli, (c) average tensile strength, and (d) average elongation to failure of the control, low, medium, and high level of hydrogen peroxide vapor treatment using 35% liquid hydrogen peroxide as the source.

In Figure *27*a, there was a visible necking behavior from the control groups of the PLA/ASA fibers. As the level of the vapor phase hydrogen peroxide treatment increased, the necking behavior became less pronounce. This finding indicated that the strengthening effect

attributed to ASA was reduced due to hydrogen peroxide vapor. In Figure *26*a, there was no necking behavior in the control groups of blank PLA fibers as well as these fibers after hydrogen peroxide vapor treatments. This observation supported the strengthening effect in the PLA/ASA fibers and the effects of hydrogen peroxide vapor treatments on the intermolecular interactions between the ASA and the PLA matrix.

For the blank PLA fibers, increasing levels of the hydrogen peroxide vapor exposure resulted in minimal changes on the average elastic moduli, suggesting no changes on the molecular configurations of the PLA matrix. However, increasing levels of the hydrogen peroxide vapor exposure on the PLA/ASA fibers decreased the average elastic moduli. Studies showed that the elastic modulus decreased when increasing the plasticizing effects [132]. This finding indicated that the hydrogen peroxide vapor affected the intermolecular bonds between the ASA and the PLA matrix. The strengthening effect attributed to the incorporation of ASA was reduced by the exposure to hydrogen peroxide vapor.

The blank PLA fibers experienced minimal changes in the average tensile strength, indicating that the semi-crystalline molecular structure of the PLA was unaltered by the hydrogen peroxide vapor treatments. However, in the PLA/ASA fibers, the control groups had a higher average tensile strength than the hydrogen peroxide vapor treatment groups. This result suggested that increasing the level of hydrogen peroxide vapor treatment caused the intermolecular bonding between the ASA and PLA to be interrupted. In other words, hydrogen peroxide vapor treatment of the PLA/ASA fibers caused a change in the molecular structure of the PLA/ASA matrix. This change promoted a plasticizing effect that has been seen in a similar study with the addition of small molecule drugs [133].

The blank PLA fibers had a decrease in the average elongation to failure for the hydrogen peroxide treatment groups as compared to the control groups. There were minimal changes on the average elongation to failure of the blank PLA fibers within the hydrogen peroxide treatment groups irrespective on the levels of hydrogen peroxide vapor exposure. Meanwhile, the average elongations to failure of the PLA/ASA fibers were significantly different ($P < 0.05$). This observation supported the finding that fiber molecular structure changed from amorphous configurations to semi-crystalline structures after various levels of hydrogen peroxide vapor treatments. In a similar study, results showed that increasing the amount of PEG 400 as a plasticizer in the polymer matrix, the elongation to failure increased briefly followed by a decrease as more PEG 400 was added to the polymer matrix [134].

5.3.5. FTIR

FTIR studies were performed on blank PLA fibers before and after various levels of hydrogen peroxide vapor concentration-time exposure to confirm the stability of the chemical structure of the polymer matrix. The low wavenumbers of the FTIR spectrum is referred to as the fingerprint region. In this region, characteristic bands related to different vibration modes of the chemical structures within the molecular chains of polymers are observed (i.e. bending and stretching) [135,136]. Due to the uniqueness of the molecular constitution of a polymer, FTIR spectra can be used to verify the molecular makeup of polymers [137]. FTIR spectroscopy is a nondestructive material characterization technique that can be used to examine the chemical structure of polymers.

The characteristic bands of PLA functional groups can be observed in Figure *28*, including C=O stretching, CH_3 asymmetrical scissoring, C-O asymmetrical stretching, C-O-C symmetrical stretching, and C-CH_3 symmetrical stretching, at 1751 cm^{-1}, 1452 cm^{-1}, 1180 cm^{-1},

1073 cm^{-1}, and 1040 cm^{-1}, respectively [138,139]. The CH_3 asymmetrical scissoring and C-CH_3 symmetrical stretching are the areas that would of underwent a shift in peaks if the hydrogen peroxide vapor altered the intramolecular bonding. However, as the levels of hydrogen peroxide vapor concentration-time exposure increased, there was no shift from these peaks. This indicated that the hydrogen peroxide vapor was not modifying or oxidizing the molecular configurations of the PLA matrix.

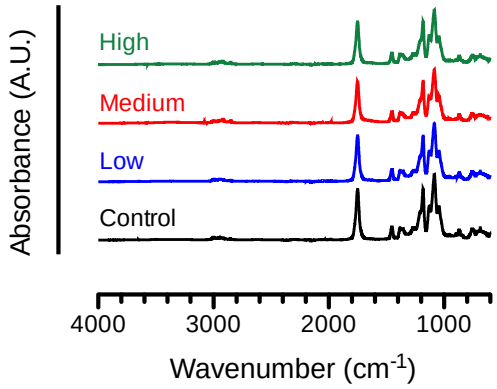

Figure 28. FTIR spectra of blank PLA fibers on the control, low, medium, and high level of hydrogen peroxide vapor treatments using 35% liquid hydrogen peroxide as the source.

5.3.6. Drug Release Assay

The drug-loaded PLA fibers were cut into 7/16" diameter discs followed by various levels of hydrogen peroxide vapor concentration-time exposure. The disc samples were then placed into a predetermined amount of PBS for in vitro drug release studies. Aliquot of liquid samples were taken at 2, 4, 8, 24 and 48 hours from the sample vials. The liquid samples were then analyzed using a UV-Vis spectrophotometer to determine the concentrations of ASA in the PBS at various time points.

The cumulative release curves of the PLA/ASA fibers after various levels of hydrogen peroxide vapor concentration-time exposure are shown in Figure *29*. As seen from the figure, ASA-loaded PLA fibers after exposure to hydrogen peroxide vapor demonstrated burst release behaviors as compared to the control groups (i.e., PLA/ASA fibers without hydrogen peroxide vapor treatment). The final cumulative release of the ASA from PLA fibers at 48 hours were 65.07 ± 4.64 %, 64.59 ± 4.13 %, 65.90 ± 3.41 %, and 70.91 ± .88 % for the control, low, medium, and high groups, respectively.

As the levels of hydrogen peroxide vapor concentration-time exposure increased, there was a tendency toward the initial burst release behavior. Furthermore, the burst release behavior increased as the levels of hydrogen peroxide vapor concentration-time exposure increased. This indicated that the hydrogen peroxide vapor was interrupting the intermolecular bonds between the ASA and the PLA matrix. A similar study found that strong interactions between fibers and water molecules facilitated a faster and more intense burst release of the small molecule drug [140]. The interruption of the intermolecular bonds between the drug molecules and the polymer matrix caused the drugs to be quickly diffused out from the core of the fibers to the surfaces, resulting in the increase in the initial release rates as the levels of hydrogen peroxide vapor concentration-time exposure increased.

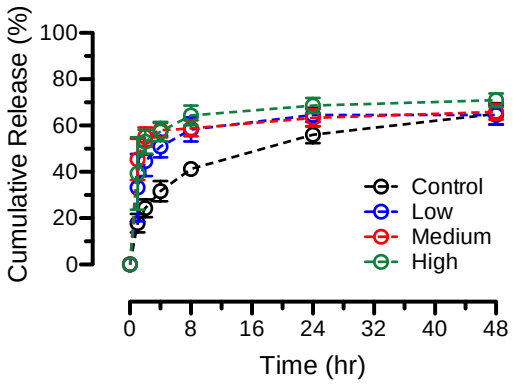

Figure 29. In vitro drug release assays of PLA/ASA fibers from control, low, medium, and high level of hydrogen peroxide vapor treatments using 35% liquid hydrogen peroxide as the source.

Chapter 6

Conclusions and Suggested Future Works

In the first part of this thesis, acetylsalicylic acid (ASA) was formulated in polymer solutions containing polylactic acid (PLA) and hexafluoroisopropanol (HFIP) at various days: PLA/ASA (1 day), PLA/ASA (14 days), and PLA/ASA (28 days), and at various drug loading percentages: PLA/ASA (15%), PLA/ASA (30%), and PLA/ASA (45%), for potential topical drug delivery applications. The stability of the ASA in HFIP showed no signs of degradation. SEM images displayed that all PLA/ASA fibers had smooth and uniform fiber surfaces with no defects. The average fiber diameter of PLA/ASA fibers showed a slight increase followed by a decrease when increasing the mixing days of ASA in HFIP. It was found that the addition of ASA into the PLA fibers produced a strengthening effect, and the strengthening effect was reduced when increasing the mixing days of ASA in HFIP. Additionally, observations from the in vitro drug release assay showed that the drug release rate changed to a burst release behavior as the mixing days of ASA in HFIP increased, demonstrating the presence of more surface drugs.

For PLA/ASA fibers at various drug loadings, PLA/ASA (15%), PLA/ASA (30%), and PLA/ASA (45%), SEM images showed no drug aggregates formed on the surface of the fibers. It was demonstrated that increasing drug loading in the PLA fibers increased the average fiber diameter and the average fiber mat density. Furthermore, results from mechanical testing indicated that the strengthening effect, produce by the intermolecular interactions of the ASA and PLA, reached a plateau due to the saturation of the molecular coupling sties. The in vitro drug release assays showed that increasing drug loading promoted the burst release behaviors.

A fiber degradation study was performed, and it was found that the mechanical properties of PLA fibers were unchanged after incubating in PBS for up to 48 hours. However, the

mechanical properties of the PLA/ASA fibers, using 1 day mixing and 15% ASA loading suggested a significant decrease of the stiffness and elongation to failure after 48 hours of drug release assays. The loss of mechanical properties was attributed to the drug release behaviors of the drug-eluting fibers.

In the second part of this thesis, a handheld vapor phase hydrogen peroxide device was designed and built to examine how various levels of concentration-time exposures affected the physico-mechanical PLA/ASA fibers. Fiber morphology and fiber mat microstructure observations suggested no degradation and no drug recrystallizations on the PLA/ASA fibers after various levels of hydrogen peroxide vapor treatments. The average fiber diameter of the PLA/ASA fibers decreased when increasing the effective exposure of the fibers to hydrogen peroxide vapor, indicating an interaction between the hydrogen peroxide vapor and its by-product of water molecules with the ASA encapsulated in the fibers. Changes on physical properties, such as area and weight of the fiber mats, were minimal for the blank PLA fibers while the PLA/ASA fibers experienced a decrease due to the vapor phase hydrogen peroxide treatments that was attributed to an increased level in hydrolysis degradation of the ASA from PLA.

In addition, mechanical properties of the PLA/ASA fibers after vapor phase hydrogen peroxide treatments suggested the alleviation of the strengthening effects due to the incorporation of the ASA in PLA fibers. FTIR analyses showed that the PLA underwent no changes in molecular configurations after vapor phase hydrogen peroxide treatments. In vitro drug release assays on PLA/ASA fibers after various levels of vapor phase hydrogen peroxide treatments showed a change to burst release behavior with the increase in the vapor phase

hydrogen peroxide exposure. This finding indicated the role of hydrogen peroxide vapor on the interruption of the intermolecular bonds between the ASA and PLA matrix.

For future work, it is suggested to perform drug release assays under mechanical loading to investigate the role of external force on the intermolecular secondary bonds between the drug and the polymer matrix. It is also suggested to include more electrospun drug-eluting fiber systems for the vapor phase hydrogen peroxide exposure to establish a database for a more comprehensive understanding on the physico-mechanical properties and materials compatibilities of drug-eluting fibers suitable for topical drug delivery systems.

References

[1] M.S. Roberts, H.S. Cheruvu, S.E. Mangion, A. Alinaghi, H.A.E. Benson, Y. Mohammed, A. Holmes, J. van der Hoek, M. Pastore, J.E. Grice, Topical drug delivery: History, percutaneous absorption, and product development, Advanced Drug Delivery Reviews. 177 (2021) 113929. https://doi.org/10.1016/j.addr.2021.113929.

[2] D. Singh Malik, N. Mital, G. Kaur, Topical drug delivery systems: A patent review, Expert Opinion on Therapeutic Patents. 26 (2016) 213–228. https://doi.org/10.1517/13543776.2016.1131267.

[3] D. Bhowmik, Gopinath,Harish, Kumar,B. Pragati, Duraivel, S., Kumar, K.P.Sampath, Recent advances in novel topical drug delivery system, The Pharma Innovation Journal. 1 (2013) 12–31. http://dx.doi.org/10.22271/tpi.

[4] M. Joshi, B.S. Butola, K. Saha, Advances in topical drug delivery system: micro to nanofibrous structures, J Nanosci Nanotechnol. 14 (2014) 853–867. https://doi.org/10.1166/jnn.2014.9083.

[5] Q. Li, X. Li, C. Zhao, Strategies to Obtain Encapsulation and Controlled Release of Small Hydrophilic Molecules, Frontiers in Bioengineering and Biotechnology. 8 (2020) 437. https://doi.org/10.3389/fbioe.2020.00437.

[6] F.W. Rost, J.M. Polak, Fluorescence microscopy and microspectrofluorimetry of malignant melanomas, naevi and normal melanocytes, Virchows Arch A Pathol Pathol Anat. 347 (1969) 321–326. https://doi.org/10.1007/bf00542675.

[7] W.A. Rutala, D.J. Weber, 301 - Disinfection, sterilization, and control of hospital waste, in: J.E. Bennett, R. Dolin, M.J. Blaser (Eds.), Mandell, Douglas, and Bennett's Principles and Practice of Infectious Diseases (Eighth Edition), Content Repository Only!, Philadelphia, 2015: pp. 3294-3309.e4. https://doi.org/10.1016/B978-1-4557-4801-3.00301-5.

[8] S. Mohapatra, Sterilization and disinfection, Essentials of Neuroanesthesia. (2017) 929–944. https://doi.org/10.1016/B978-0-12-805299-0.00059-2.

[9] J.M. Boyce, A review of wipes used to disinfect hard surfaces in health care facilities, American Journal of Infection Control. 49 (2021) 104–114. https://doi.org/10.1016/j.ajic.2020.06.183.

[10] G. Moccia, O. Motta, C. Pironti, A. Proto, M. Capunzo, F. De Caro, An alternative approach for the decontamination of hospital settings, Journal of Infection and Public Health. 13 (2020) 2038–2044. https://doi.org/10.1016/j.jiph.2020.09.020.

[11] D.J. Weber, W.A. Rutala, E.E. Sickbert-Bennett, H. Kanamori, D. Anderson, Continuous room decontamination technologies, American Journal of Infection Control. 47 (2019) A72–A78. https://doi.org/10.1016/j.ajic.2019.03.016.

[12] J.G. Solon, S. Killeen, Decontamination and sterilization, Surgery (Oxford). 37 (2019) 51–57. https://doi.org/10.1016/j.mpsur.2018.11.002.

[13] H.F. Bohner, R.L. Bradley, Corrosivity of chlorine dioxide used as sanitizer in ultrafiltration systems, Journal of Dairy Science. 74 (1991) 3348–3352. https://doi.org/10.3168/jds.S0022-0302(91)78523-8.

[14] J.A. Otter, S. Yezli, T.M. Perl, F. Barbut, G.L. French, 17 - A guide to no-touch automated room disinfection (NTD) systems, in: J.T. Walker (Ed.), Decontamination in

Hospitals and Healthcare, Woodhead Publishing, 2014: pp. 413–460. https://doi.org/10.1533/9780857096692.2.413.
[15] T. Pottage, J.T. Walker, 12 - Use of gaseous decontamination technologies for wards and isolation rooms in hospitals and healthcare settings, in: Decontamination in Hospitals and Healthcare, Woodhead Publishing, 2014: pp. 299–324. https://doi.org/10.1533/9780857096692.2.299.
[16] Y. Dang, J. Guan, Nanoparticle-based drug delivery systems for cancer therapy, Smart Materials in Medicine. 1 (2020) 10–19. https://doi.org/10.1016/j.smaim.2020.04.001.
[17] M.D. Buhecha, A.B. Lansley, S. Somavarapu, A.S. Pannala, Development and characterization of PLA nanoparticles for pulmonary drug delivery: Co-encapsulation of theophylline and budesonide, a hydrophilic and lipophilic drug, Journal of Drug Delivery Science and Technology. 53 (2019) 101128. https://doi.org/10.1016/j.jddst.2019.101128.
[18] M. Al Malyan, C. Becchi, L. Nikkola, P. Viitanen, S. Boncinelli, F. Chiellini, N. Ashammakhi, Polymer-based biodegradable drug delivery systems in pain management, J Craniofac Surg. 17 (2006) 302–313. https://doi.org/10.1097/00001665-200603000-00018.
[19] S. Barbieri, F. Buttini, A. Rossi, R. Bettini, P. Colombo, G. Ponchel, F. Sonvico, G. Colombo, Ex vivo permeation of tamoxifen and its 4-OH metabolite through rat intestine from lecithin/chitosan nanoparticles, International Journal of Pharmaceutics. 491 (2015) 99–104. https://doi.org/10.1016/j.ijpharm.2015.06.021.
[20] S. Liu, S. Yang, P.C. Ho, Intranasal administration of carbamazepine-loaded carboxymethyl chitosan nanoparticles for drug delivery to the brain, Asian Journal of Pharmaceutical Sciences. 13 (2018) 72–81. https://doi.org/10.1016/j.ajps.2017.09.001.
[21] S.K. Pandey, S. Ghosh, P. Maiti, C. Haldar, Therapeutic efficacy and toxicity of tamoxifen loaded PLA nanoparticles for breast cancer, International Journal of Biological Macromolecules. 72 (2015) 309–319. https://doi.org/10.1016/j.ijbiomac.2014.08.012.
[22] K.T. Householder, D.M. DiPerna, E.P. Chung, G.M. Wohlleb, H.D. Dhruv, M.E. Berens, R.W. Sirianni, Intravenous delivery of camptothecin-loaded PLGA nanoparticles for the treatment of intracranial glioma, International Journal of Pharmaceutics. 479 (2015) 374–380. https://doi.org/10.1016/j.ijpharm.2015.01.002.
[23] A. Nagalingam, Chapter 15 - Drug delivery aspects of herbal medicines, in: S. Arumugam, K. Watanabe (Eds.), Japanese Kampo Medicines for the Treatment of Common Diseases: Focus on Inflammation, Academic Press, 2017: pp. 143–164. https://doi.org/10.1016/B978-0-12-809398-6.00015-9.
[24] R. Sonkar, Sonali, A. Jha, M.K. Viswanadh, A.S. Burande, Narendra, D.M. Pawde, K.K. Patel, M. Singh, B. Koch, M.S. Muthu, Gold liposomes for brain-targeted drug delivery: Formulation and brain distribution kinetics, Materials Science and Engineering: C. 120 (2021) 111652. https://doi.org/10.1016/j.msec.2020.111652.
[25] M. Huang, Y. Pu, Y. Peng, Q. Fu, L. Guo, Y. Wu, Y. Zheng, Biotin and glucose dual-targeting, ligand-modified liposomes promote breast tumor-specific drug delivery, Bioorganic & Medicinal Chemistry Letters. 30 (2020) 127151. https://doi.org/10.1016/j.bmcl.2020.127151.
[26] E.M. Ahmed, Hydrogel: preparation, characterization, and applications: A review, Journal of Advanced Research. 6 (2015) 105–121. https://doi.org/10.1016/j.jare.2013.07.006.

[27] K. Pal, A.K. Banthia, D.K. Majumdar, Polymeric hydrogels: Characterization and biomedical applications, Designed Monomers and Polymers. 12 (2009) 197–220. https://doi.org/10.1163/156855509X436030.
[28] Y. Liang, K.L. Kiick, Liposome-cross-linked hybrid hydrogels for glutathione-triggered delivery of multiple cargo molecules, Biomacromolecules. 17 (2016) 601–614. https://doi.org/10.1021/acs.biomac.5b01541.
[29] P. Zhang, L. He, J. Zhang, X. Mei, Y. Zhang, H. Tian, Z. Chen, Preparation of novel berberine nano-colloids for improving wound healing of diabetic rats by acting Sirt1/NF-κB pathway, Colloids and Surfaces B: Biointerfaces. 187 (2020) 110647. https://doi.org/10.1016/j.colsurfb.2019.110647.
[30] M.-T. Sheu, H.-J. Jhan, C.-Y. Su, L.-C. Chen, C.-E. Chang, D.-Z. Liu, H.-O. Ho, Codelivery of doxorubicin-containing thermosensitive hydrogels incorporated with docetaxel-loaded mixed micelles enhances local cancer therapy, Colloids and Surfaces B: Biointerfaces. 143 (2016) 260–270. https://doi.org/10.1016/j.colsurfb.2016.03.054.
[31] D.G. Leach, N. Dharmaraj, S.L. Piotrowski, T.L. Lopez-Silva, Y.L. Lei, A.G. Sikora, S. Young, J.D. Hartgerink, STINGel: Controlled release of a cyclic dinucleotide for enhanced cancer immunotherapy, Biomaterials. 163 (2018) 67–75. https://doi.org/10.1016/j.biomaterials.2018.01.035.
[32] H. Janik, M. Marzec, A review: Fabrication of porous polyurethane scaffolds, Materials Science and Engineering: C. 48 (2015) 586–591. https://doi.org/10.1016/j.msec.2014.12.037.
[33] D.K. Patel, S.D. Dutta, K. Ganguly, K.-T. Lim, Multifunctional bioactive chitosan/cellulose nanocrystal scaffolds eradicate bacterial growth and sustain drug delivery, International Journal of Biological Macromolecules. 170 (2021) 178–188. https://doi.org/10.1016/j.ijbiomac.2020.12.145.
[34] P.X. Ma, Scaffolds for tissue fabrication, Materials Today. 7 (2004) 30–40. https://doi.org/10.1016/S1369-7021(04)00233-0.
[35] A. Jadidi, E. Salahinejad, E. Sharifi, L. Tayebi, Drug-delivery Ca-Mg silicate scaffolds encapsulated in PLGA, International Journal of Pharmaceutics. 589 (2020) 119855. https://doi.org/10.1016/j.ijpharm.2020.119855.
[36] I. Cantón, R. Mckean, M. Charnley, K.A. Blackwood, C. Fiorica, A.J. Ryan, S. MacNeil, Development of an ibuprofen-releasing biodegradable PLA/PGA electrospun scaffold for tissue regeneration, Biotechnology and Bioengineering. 105 (2010) 396–408. https://doi.org/10.1002/bit.22530.
[37] E. Zdraveva, J. Fang, B. Mijovic, T. Lin, 11 - Electrospun nanofibers, in: G. Bhat (Ed.), Structure and Properties of High-Performance Fibers, Woodhead Publishing, Oxford, 2017: pp. 267–300. https://doi.org/10.1016/B978-0-08-100550-7.00011-5.
[38] Q. Wei, D. Tao, Y. Xu, 1 - Nanofibers: principles and manufacture, in: Q. Wei (Ed.), Functional Nanofibers and Their Applications, Woodhead Publishing, 2012: pp. 3–21. https://doi.org/10.1533/9780857095640.1.1.
[39] S. Kajdič, O. Planinšek, M. Gašperlin, P. Kocbek, Electrospun nanofibers for customized drug-delivery systems, Journal of Drug Delivery Science and Technology. 51 (2019) 672–681. https://doi.org/10.1016/j.jddst.2019.03.038.
[40] M.A. Mohamady Hussein, E. Guler, E. Rayaman, M.E. Cam, A. Sahin, M. Grinholc, D. Sezgin Mansuroglu, Y.M. Sahin, O. Gunduz, M. Muhammed, I.M. El-Sherbiny, M.

Megahed, Dual-drug delivery of Ag-chitosan nanoparticles and phenytoin via core-shell PVA/PCL electrospun nanofibers, Carbohydrate Polymers. 270 (2021) 118373. https://doi.org/10.1016/j.carbpol.2021.118373.
[41] P. Zahedi, Z. Karami, I. Rezaeian, S.-H. Jafari, P. Mahdaviani, A.H. Abdolghaffari, M. Abdollahi, Preparation and performance evaluation of tetracycline hydrochloride loaded wound dressing mats based on electrospun nanofibrous poly(lactic acid)/poly(ϵ-caprolactone) blends, Journal of Applied Polymer Science. 124 (2012) 4174–4183. https://doi.org/10.1002/app.35372.
[42] C.-W. Chang, W.-C. Lai, A strategy for preparing solid polymer electrolytes via the electrospinning process, Journal of the Taiwan Institute of Chemical Engineers. 116 (2020) 279–285. https://doi.org/10.1016/j.jtice.2020.11.012.
[43] Electrospinning process and applications of electrospun fibers, Journal of Electrostatics. 35 (1995) 151–160. https://doi.org/10.1016/0304-3886(95)00041-8.
[44] N. Angel, L. Guo, F. Yan, H. Wang, L. Kong, Effect of processing parameters on the electrospinning of cellulose acetate studied by response surface methodology, Journal of Agriculture and Food Research. 2 (2020) 100015. https://doi.org/10.1016/j.jafr.2019.100015.
[45] N. Aliheidari, N. Aliahmad, M. Agarwal, H. Dalir, Electrospun nanofibers for label-free sensor applications, Sensors. 19 (2019) 3587. https://doi.org/10.3390/s19163587.
[46] M.S. Singhvi, S.S. Zinjarde, D.V. Gokhale, Polylactic acid: Synthesis and biomedical applications, Journal of Applied Microbiology. 127 (2019) 1612–1626. https://doi.org/10.1111/jam.14290.
[47] A. Jain, W. Khan, A. Kyzioł, Chapter 10 - Particulate systems of PLA and its copolymers, in: V. Grumezescu, A.M. Grumezescu (Eds.), Materials for Biomedical Engineering, Elsevier, 2019: pp. 349–380. https://doi.org/10.1016/B978-0-12-816874-5.00010-4.
[48] R.P. Pawar, S.U. Tekale, S.U. Shisodia, J.T. Totre, A.J. Domb, Biomedical applications of poly(lactic acid), Recent Patents on Regenerative Medicine. 4 (2014) 40–51. https://doi.org/10.2174/22102965046661404022350 24.
[49] N.F. Zaaba, M. Jaafar, A review on degradation mechanisms of polylactic acid: Hydrolytic, photodegradative, microbial, and enzymatic degradation, Polymer Engineering & Science. 60 (2020) 2061–2075. https://doi.org/10.1002/pen.25511.
[50] K.I. Park, M. Xanthos, A study on the degradation of polylactic acid in the presence of phosphonium ionic liquids, Polymer Degradation and Stability. 94 (2009) 834–844. https://doi.org/10.1016/j.polymdegradstab.2009.01.030.
[51] I.S.M.A. Tawakkal, M.J. Cran, J. Miltz, S.W. Bigger, A review of poly(lactic acid)-Based materials for antimicrobial packaging, Journal of Food Science. 79 (2014) 1477–1490. https://doi.org/10.1111/1750-3841.12534.
[52] A. Belbella, C. Vauthier, H. Fessi, J.-P. Devissaguet, F. Puisieux, In vitro degradation of nanospheres from poly(D,L-lactides) of different molecular weights and polydispersities, International Journal of Pharmaceutics. 129 (1996) 95–102. https://doi.org/10.1016/0378-5173(95)04258-X.
[53] C. Nicolae, M. Grigorescu, R. Gabor, An investigation of thermal degradation of poly(lactic acid), Engineering Letters. 16 (2008) 568–571. https://doi.org/10.1.1.148.7599.
[54] S.-H. Hyon, K. Jamshidi, Y. Ikada, Melt Spinning of Poly-L-Lactide and Hydrolysis of the Fiber in Vitro, in: S.W. Shalaby, A.S. Hoffman, B.D. Ratner, T.A. Horbett (Eds.),

Polymers as Biomaterials, Springer US, Boston, MA, 1984: pp. 51–65. https://doi.org/10.1007/978-1-4613-2433-1_5.
[55] F. Alexis, Factors affecting the degradation and drug-release mechanism of poly(lactic acid) and poly[(lactic acid)-co-(glycolic acid)], Polymer International. 54 (2005) 36–46. https://doi.org/10.1002/pi.1697.
[56] J. Izdebska, 22 - Aging and degradation of printed materials, in: J. Izdebska, S. Thomas (Eds.), Printing on Polymers, William Andrew Publishing, 2016: pp. 353–370. https://doi.org/10.1016/B978-0-323-37468-2.00022-1.
[57] S. Farah, D.G. Anderson, R. Langer, Physical and mechanical properties of PLA, and their functions in widespread applications — A comprehensive review, Advanced Drug Delivery Reviews. 107 (2016) 367–392. https://doi.org/10.1016/j.addr.2016.06.012.
[58] H. Tsuji, Y. Ikada, Properties and morphology of poly(l-lactide) 4. Effects of structural parameters on long-term hydrolysis of poly(l-lactide) in phosphate-buffered solution, Polymer Degradation and Stability. 67 (2000) 179–189. https://doi.org/10.1016/S0141-3910(99)00111-1.
[59] A.G. Ríos-Castillo, F.F. Umaña, J.J. Rodríguez-Jerez, Long-term antibacterial efficacy of disinfectants based on benzalkonium chloride and sodium hypochlorite tested on surfaces against resistant gram-positive bacteria, Food Control. 93 (2018) 219–225. https://doi.org/10.1016/j.foodcont.2018.06.008.
[60] S. Tiwari, S. Rajak, D.P. Mondal, D. Biswas, Sodium hypochlorite is more effective than 70% ethanol against biofilms of clinical isolates of staphylococcus aureus, American Journal of Infection Control. 46 (2018) e37–e42. https://doi.org/10.1016/j.ajic.2017.12.015.
[61] A.P. Fraise, Choosing disinfectants, Journal of Hospital Infection. 43 (1999) 255–264. https://doi.org/10.1016/S0195-6701(99)90421-8.
[62] L.A. Jury, J.L. Cadnum, A. Jennings-Sanders, E.C. Eckstein, S. Chang, C.J. Donskey, Evaluation of an alcohol-based power sanitizing system for decontamination of hospital rooms of patients with methicillin-resistant staphylococcus aureus carriage, American Journal of Infection Control. 38 (2010) 234–236. https://doi.org/10.1016/j.ajic.2009.09.011.
[63] M. Best, V.S. Springthorpe, S.A. Sattar, Feasibility of a combined carrier test for disinfectants: studies with a mixture of five types of microorganisms, American Journal of Infection Control. 22 (1994) 152–162. https://doi.org/10.1016/0196-6553(94)90004-3.
[64] H. Celebi, E.B. Büyükerkmen, E. Torlak, Disinfection of polyvinyl siloxane impression material by gaseous ozone, The Journal of Prosthetic Dentistry. 120 (2018) 138–143. https://doi.org/10.1016/j.prosdent.2017.09.003.
[65] M.S. Lopes, J.R.F. Ferreira, K.B. da Silva, I. de Oliveira Bacelar Simplício, C.J. de Lima, A.B. Fernandes, Disinfection of corrugated tubing by ozone and ultrasound in mechanically ventilated tracheostomized patients, Journal of Hospital Infection. 90 (2015) 304–309. https://doi.org/10.1016/j.jhin.2015.03.004.
[66] W.J. Kowalski, W.P. Bahnfleth, T.S. Whittam, Bactericidal effects of high airborne ozone concentrations on escherichia coli and staphylococcus aureus, Ozone: Science & Engineering. 20 (1998) 205–221. https://doi.org/10.1080/01919519808547272.

[67] B. Palcsó, Z. Moldován, K. Süvegh, A. Herczegh, R. Zelkó, Chlorine dioxide-loaded poly(acrylic acid) gels for prolonged antimicrobial effect, Materials Science and Engineering: C. 98 (2019) 782–788. https://doi.org/10.1016/j.msec.2019.01.043.
[68] 1988 OSHA PEL Project - Chlorine Dioxide | NIOSH | CDC, (2020). https://www.cdc.gov/niosh/pel88/10049-04.html (accessed August 11, 2020).
[69] C.P. Chauret, Sanitization, in: C.A. Batt, M.L. Tortorello (Eds.), Encyclopedia of Food Microbiology (Second Edition), Academic Press, Oxford, 2014: pp. 360–364. https://doi.org/10.1016/B978-0-12-384730-0.00407-9.
[70] S.T. Ahmed, A.B.M.R. Bostami, H.-S. Mun, C.-J. Yang, Efficacy of chlorine dioxide gas in reducing Escherichia coli and Salmonella from broiler house environments, Journal of Applied Poultry Research. 26 (2017) 84–88. https://doi.org/10.3382/japr/pfw048.
[71] G. Izmirlioglu, B. Ouyang, A. Demirci, Utilization of pulsed UV light for inactivation of salmonella enteritidis on shelled walnuts, LWT. (2020) 110023. https://doi.org/10.1016/j.lwt.2020.110023.
[72] M. Lindblad, E. Tano, C. Lindahl, F. Huss, Ultraviolet-C decontamination of a hospital room: Amount of UV light needed, Burns. 46 (2020) 842–849. https://doi.org/10.1016/j.burns.2019.10.004.
[73] T. Sandle, 9 - Hydrogen peroxide vapour sterilisation, in: T. Sandle (Ed.), Sterility, Sterilisation and Sterility Assurance for Pharmaceuticals, Woodhead Publishing, 2013: pp. 129–141. https://doi.org/10.1533/9781908818638.129.
[74] G. Fey, S. Klassen, S. Theriault, J. Krishnan, Decontamination of a worst-case scenario class II biosafety cabinet using vaporous hydrogen peroxide, Appl Biosaf. 15 (2010) 142–150. https://doi.org/10.1177/153567601001500307.
[75] ATSDR - ToxFAQs^{TM}: Hydrogen Peroxide, (n.d.). https://www.atsdr.cdc.gov/toxfaqs/tf.asp?id=305&tid=55 (accessed May 14, 2020).
[76] L. Ernstgård, B. Sjögren, G. Johanson, Acute effects of exposure to vapors of hydrogen peroxide in humans, Toxicology Letters. 212 (2012) 222–227. https://doi.org/10.1016/j.toxlet.2012.05.025.
[77] PubChem, Hydrogen peroxide, (n.d.). https://pubchem.ncbi.nlm.nih.gov/compound/784 (accessed September 3, 2020).
[78] The Effects of Heating H_2O_2 and Stability, Sciencing. (n.d.). https://sciencing.com/effects-heating-h2o2-stability-6187449.html (accessed September 3, 2020).
[79] T.Y. Fu, P. Gent, V. Kumar, Efficacy, efficiency and safety aspects of hydrogen peroxide vapour and aerosolized hydrogen peroxide room disinfection systems, Journal of Hospital Infection. 80 (2012) 199–205. https://doi.org/10.1016/j.jhin.2011.11.019.
[80] M.Á. Gómez García, I. Dobrosz-Gómez, J.C. Ojeda Toro, Thermal safety assessment for catalytic decomposition of hydrogen peroxide by dynamic analysis, Process Safety and Environmental Protection. 109 (2017) 46–54. https://doi.org/10.1016/j.psep.2017.03.025.
[81] X. Jia, F. Sun, Y. Fei, M. Jin, F. Zhang, W. Xu, N. Shi, Z. Lv, Explosion characteristics of mixtures containing hydrogen peroxide and working solution in the anthraquinone route to hydrogen peroxide, Process Safety and Environmental Protection. 119 (2018) 218–222. https://doi.org/10.1016/j.psep.2018.08.007.
[82] W.F. Gale, N.I. Sofyan, H.S. Gale, M.H. Sk, S.-F. Chou, J.W. Fergus, C.G. Shannon, Effect of vapour phase hydrogen peroxide, as a decontaminant for civil aviation applications, on microstructure, tensile properties and corrosion resistance of 2024 and

7075 age hardenable aluminium alloys and 304 austenitic stainless steel, Materials Science and Technology. 25 (2009) 76–84. https://doi.org/10.1179/174328408X307256.
[83] S.F. Chou, R.A. Overfelt, W.F. Gale, H.S. Gale, C.G. Shannon, G. Buschle-Diller, J. Watson, Effects of Hydrogen Peroxide on Common Aviation Textiles, (n.d.) 30.
[84] W. Anna, G. Beata, R. Dorota, P. Katarzyna, M. Waldemar, W. Henryk, P. Aleksandra, W. Anetta, O. Anna, S. Justyna, A. Justyna, Vapourised hydrogen peroxide (VHP) and ethylene oxide (EtO) methods for disinfecting historical cotton textiles from the Auschwitz-Birkenau State Museum in Oświęcim, Poland, International Biodeterioration & Biodegradation. 133 (2018) 42–51. https://doi.org/10.1016/j.ibiod.2018.05.016.
[85] S.M. Loo, J. Kiepert, D. Klein, M. Pook, S.-F. Chou, T. Overfelt, J. Watson, Evaluation of the effects of hydrogen peroxide on common aircraft electrical materials, (n.d.) 22. https://doi.org/DOT/FAA/AM-10/5.
[86] T. Pottage, J.T. Walker, 12 - Use of gaseous decontamination technologies for wards and isolation rooms in hospitals and healthcare settings, in: J.T. Walker (Ed.), Decontamination in Hospitals and Healthcare, Woodhead Publishing, 2014: pp. 299–324. https://doi.org/10.1533/9780857096692.2.299.
[87] F. Barbut, S. Yezli, J.A. Otter, Activity in vitro of hydrogen peroxide vapour against Clostridium difficile spores, Journal of Hospital Infection. 80 (2012) 85–87. https://doi.org/10.1016/j.jhin.2011.10.005.
[88] S. Shapey, K. Machin, K. Levi, T.C. Boswell, Activity of a dry mist hydrogen peroxide system against environmental clostridium difficile contamination in elderly care wards, Journal of Hospital Infection. 70 (2008) 136–141. https://doi.org/10.1016/j.jhin.2008.06.008.
[89] J. McCord, M. Prewitt, E. Dyakova, S. Mookerjee, J.A. Otter, Reduction in clostridium difficile infection associated with the introduction of hydrogen peroxide vapour automated room disinfection, Journal of Hospital Infection. 94 (2016) 185–187. https://doi.org/10.1016/j.jhin.2016.05.014.
[90] J.A. Otter, S. Yezli, M.A. Schouten, A.R.H. van Zanten, G. Houmes-Zielman, M.K.E. Nohlmans-Paulssen, Hydrogen peroxide vapor decontamination of an intensive care unit to remove environmental reservoirs of multidrug-resistant gram-negative rods during an outbreak, American Journal of Infection Control. 38 (2010) 754–756. https://doi.org/10.1016/j.ajic.2010.03.010.
[91] J.A. Otter, S. Yezli, G.L. French, Impact of the suspending medium on susceptibility of meticillin-resistant staphylococcus aureus to hydrogen peroxide vapour decontamination, Journal of Hospital Infection. 82 (2012) 213–215. https://doi.org/10.1016/j.jhin.2012.08.006.
[92] S. Ali, M. Muzslay, M. Bruce, A. Jeanes, G. Moore, A.P.R. Wilson, Efficacy of two hydrogen peroxide vapour aerial decontamination systems for enhanced disinfection of meticillin-resistant Staphylococcus aureus, Klebsiella pneumoniae and Clostridium difficile in single isolation rooms, Journal of Hospital Infection. 93 (2016) 70–77. https://doi.org/10.1016/j.jhin.2016.01.016.
[93] G.L. French, J.A. Otter, K.P. Shannon, N.M.T. Adams, D. Watling, M.J. Parks, Tackling contamination of the hospital environment by methicillin-resistant staphylococcus aureus (MRSA): A comparison between conventional terminal cleaning and hydrogen peroxide

vapour decontamination, Journal of Hospital Infection. 57 (2004) 31–37. https://doi.org/10.1016/j.jhin.2004.03.006.
[94] A. Jeanes, G. Rao, M. Osman, P. Merrick, Eradication of persistent environmental MRSA, Journal of Hospital Infection. 61 (2005) 85–86. https://doi.org/10.1016/j.jhin.2005.01.001.
[95] K.J. Hardy, S. Gossain, N. Henderson, C. Drugan, B.A. Oppenheim, F. Gao, P.M. Hawkey, Rapid recontamination with MRSA of the environment of an intensive care unit after decontamination with hydrogen peroxide vapour, Journal of Hospital Infection. 66 (2007) 360–368. https://doi.org/10.1016/j.jhin.2007.05.009.
[96] M. Dryden, R. Parnaby, S. Dailly, T. Lewis, K. Davis-Blues, J.A. Otter, A.M. Kearns, Hydrogen peroxide vapour decontamination in the control of a polyclonal meticillin-resistant Staphylococcus aureus outbreak on a surgical ward, Journal of Hospital Infection. 68 (2008) 190–192. https://doi.org/10.1016/j.jhin.2007.11.003.
[97] J.A. Otter, M. Cummins, F. Ahmad, C. van Tonder, Y.J. Drabu, Assessing the biological efficacy and rate of recontamination following hydrogen peroxide vapour decontamination, Journal of Hospital Infection. 67 (2007) 182–188. https://doi.org/10.1016/j.jhin.2007.07.019.
[98] J.A. Otter, S. Mepham, B. Athan, D. Mack, R. Smith, M. Jacobs, S. Hopkins, Terminal decontamination of the royal free london's high-level isolation unit after a case of ebola virus disease using hydrogen peroxide vapor, American Journal of Infection Control. 44 (2016) 233–235. https://doi.org/10.1016/j.ajic.2015.08.025.
[99] R. Casasola, N.L. Thomas, A. Trybala, S. Georgiadou, Electrospun poly lactic acid (PLA) fibres: Effect of different solvent systems on fibre morphology and diameter, Polymer. 55 (2014) 4728–4737. https://doi.org/10.1016/j.polymer.2014.06.032.
[100] C. Huang, N.L. Thomas, Fabricating porous poly(lactic acid) fibres via electrospinning, European Polymer Journal. 99 (2018) 464–476. https://doi.org/10.1016/j.eurpolymj.2017.12.025.
[101] D. Wang, Z. Sun, J. Sun, F. Liu, L. Du, D. Wang, Preparation and characterization of polylactic acid nanofiber films loading Perilla essential oil for antibacterial packaging of chilled chicken, International Journal of Biological Macromolecules. 192 (2021) 379–388. https://doi.org/10.1016/j.ijbiomac.2021.09.190.
[102] A.A.M. Zubir, M.P. Khairunnisa, N.A. Surib, J. NorRuwaida, A.H. bin M. Ali, M. Rashid, Electrospinning of PLA with DMF: Effect of polymer concentration on the bead diameter of the electrospun fibre, IOP Conf. Ser.: Mater. Sci. Eng. 778 (2020) 012087. https://doi.org/10.1088/1757-899X/778/1/012087.
[103] Z. Zhang, S.H. Lee, C.W. Gan, S.-S. Feng, In Vitro and In Vivo Investigation on PLA–TPGS Nanoparticles for Controlled and Sustained Small Molecule Chemotherapy, Pharm Res. 25 (2008) 1925–1935. https://doi.org/10.1007/s11095-008-9611-6.
[104] J. Wang, H. Zhao, K. Zhi, X. Yang, Exploration of the Natural Active Small-Molecule Drug-Loading Process and Highly Efficient Synergistic Antitumor Efficacy, ACS Appl. Mater. Interfaces. 12 (2020) 6827–6839. https://doi.org/10.1021/acsami.9b18443.
[105] ASTM Standard D1708-96: Test method for tensile properties of plastics by use of microtensile specimens, (2002). https://www.astm.org/DATABASE.CART/HISTORICAL/D1708-96.htm.
[106] ASTM Standard D882-18: Test method for tensile properties of thin plastic sheeting, (2018). https://www.astm.org/Standards/D882.

[107] P.E. Alves, B.G. Soares, L.C. Lins, S. Livi, E.P. Santos, Controlled delivery of dexamethasone and betamethasone from PLA electrospun fibers: A comparative study, European Polymer Journal. 117 (2019) 1–9. https://doi.org/10.1016/j.eurpolymj.2019.05.001.
[108] A. Dasari, J. Quirós, B. Herrero, K. Boltes, E. García-Calvo, R. Rosal, Antifouling membranes prepared by electrospinning polylactic acid containing biocidal nanoparticles, Journal of Membrane Science. 405–406 (2012) 134–140. https://doi.org/10.1016/j.memsci.2012.02.060.
[109] X. Liao, W. Xu, Y. Wang, B. Jia, G. Zhou, Effect of porous structure on mechanical properties of C/PLA/nano-HA composites scaffold, Transactions of Nonferrous Metals Society of China. 19 (2009) s748–s751. https://doi.org/10.1016/S1003-6326(10)60144-6.
[110] C.D.L. Johnson, A.R. D'Amato, R.J. Gilbert, Electrospun fibers for drug delivery after spinal cord injury and the effects of drug incorporation on fiber properties, Cells, Tissues, Organs. 202 (2016) 116. https://doi.org/10.1159/000446621.
[111] R. Malik, T. Garg, A.K. Goyal, G. Rath, Polymeric nanofibers: targeted gastro-retentive drug delivery systems, Journal of Drug Targeting. 23 (2015) 109–124. https://doi.org/10.3109/1061186X.2014.965715.
[112] P. Taepaiboon, U. Rungsardthong, P. Supaphol, Drug-loaded electrospun mats of poly(vinyl alcohol) fibres and their release characteristics of four model drugs, Nanotechnology. 17 (2006) 2317–2329. https://doi.org/10.1088/0957-4484/17/9/041.
[113] W.J. Jackson, J.R. Caldwell, Antiplasticization. II. Characteristics of antiplasticizers, Journal of Applied Polymer Science. 11 (1967) 211–226. https://doi.org/10.1002/app.1967.070110205.
[114] S.P. Chamarthy, R. Pinal, Plasticizer concentration and the performance of a diffusion-controlled polymeric drug delivery system, Colloids and Surfaces A: Physicochemical and Engineering Aspects. 331 (2008) 25–30. https://doi.org/10.1016/j.colsurfa.2008.05.047.
[115] C.L. Huang, T.W. Steele, E. Widjaja, F.Y. Boey, S.S. Venkatraman, J.S. Loo, The influence of additives in modulating drug delivery and degradation of PLGA thin films, NPG Asia Materials. 5 (2013) e54–e54. https://doi.org/10.1038/am.2013.26.
[116] C.L. Jennings, T.D. Dziubla, D.A. Puleo, Combined effects of drugs and plasticizers on the properties of drug delivery films, Journal of Bioactive and Compatible Polymers. 31 (2016) 323–333. https://doi.org/10.1177/0883911515627178.
[117] S.E. Vidotti, A.C. Chinellato, L.A. Pessan, Effects of antiplasticization on the thermal, volumetric, and transport properties of polyethersulfone, Journal of Applied Polymer Science. 103 (2007) 2627–2633. https://doi.org/10.1002/app.25371.
[118] C.L. Rabek, R.V. Stelle, T.D. Dziubla, D.A. Puleo, The effect of plasticizers on the erosion and mechanical properties of polymeric films, J Biomater Appl. 28 (2014) 10.1177/0885328213480979. https://doi.org/10.1177/0885328213480979.
[119] A. Kumar, J. Pillai, Chapter 13 - Implantable drug delivery systems: An overview, in: A.M. Grumezescu (Ed.), Nanostructures for the Engineering of Cells, Tissues and Organs, William Andrew Publishing, 2018: pp. 473–511. https://doi.org/10.1016/B978-0-12-813665-2.00013-2.
[120] S.C. Chen, X.B. Huang, X.M. Cai, J. Lu, J. Yuan, J. Shen, The influence of fiber diameter of electrospun poly(lactic acid) on drug delivery, Fibers Polym. 13 (2012) 1120–1125. https://doi.org/10.1007/s12221-012-1120-x.

[121] C. Berkland, M. King, A. Cox, K. (Kevin) Kim, D.W. Pack, Precise control of PLG microsphere size provides enhanced control of drug release rate, Journal of Controlled Release. 82 (2002) 137–147. https://doi.org/10.1016/S0168-3659(02)00136-0.
[122] Z. Huo, Y. Qiu, Z. Chu, P. Yin, W. Lu, Y. Yan, N. Wan, Z. Chen, Electrospinning preparation of timosaponin b-II-loaded PLLA nanofibers and their antitumor recurrence activities in vivo, Journal of Nanomaterials. 2015 (2015) e367964. https://doi.org/10.1155/2015/367964.
[123] Y. Zhu, M. Pyda, P. Cebe, Electrospun fibers of poly(l-lactic acid) containing lovastatin with potential applications in drug delivery, Journal of Applied Polymer Science. 134 (2017) 45287. https://doi.org/10.1002/app.45287.
[124] X. Yuan, A.F.T. Mak, K. Yao, Comparative observation of accelerated degradation of poly(l-lactic acid) fibres in phosphate buffered saline and a dilute alkaline solution, Polymer Degradation and Stability. 75 (2002) 45–53. https://doi.org/10.1016/S0141-3910(01)00203-8.
[125] S.-F. Chou, K.A. Woodrow, Relationships between mechanical properties and drug release from electrospun fibers of PCL and PLGA blends, Journal of the Mechanical Behavior of Biomedical Materials. 65 (2017) 724–733. https://doi.org/10.1016/j.jmbbm.2016.09.004.
[126] VIM-GLO-EN-H2O2-Humidity-measurements-and-hydrogen-peroxide-B212110EN-A.pdf, (n.d.). https://www.vaisala.com/sites/default/files/documents/VIM-GLO-EN-H2O2-Humidity-measurements-and-hydrogen-peroxide-B212110EN-A.pdf (accessed June 28, 2021).
[127] D. Watling, C. Ryle, M. Parks, M. Christopher, Theoretical analysis of the condensation of hydrogen peroxide gas and water vapour as used in surface decontamination, PDA Journal of Pharmaceutical Science and Technology. 56 (2002) 291–299.
[128] R.M. Shaffstall, R.P. Garner, J. Bishop, L. Cameron-Landis, D.L. Eddington, G. Hau, S. Spera, T. Mielnik, J.A. Thomas, Vaporized Hydrogen Peroxide (VHP®) Decontamination of a Section of a Boeing 747 Cabin, (n.d.) 16.
[129] S.-F. Chou, Effect of water and hydrogen peroxide on the mechanical properties and microstructure of selected natural and synthetic polymer structures, Ph.D., Auburn University, n.d. https://www.proquest.com/docview/927927665/abstract/362B1C62DF3540DBPQ/1 (accessed June 6, 2021).
[130] E.S. Trofimchuk, M.A. Moskvina, N.I. Nikonorova, A.V. Efimov, E.S. Garina, T.E. Grokhovskaya, O.A. Ivanova, A.V. Bakirov, N.G. Sedush, S.N. Chvalun, Hydrolytic degradation of polylactide films deformed by the environmental crazing mechanism, European Polymer Journal. 139 (2020) 110000. https://doi.org/10.1016/j.eurpolymj.2020.110000.
[131] PubChem, Aspirin, (n.d.). https://pubchem.ncbi.nlm.nih.gov/compound/2244 (accessed July 17, 2021).
[132] Influence of water soluble and insoluble plasticizers on the physical and mechanical properties of acrylic resin copolymers, International Journal of Pharmaceutics. 103 (1994) 293–301. https://doi.org/10.1016/0378-5173(94)90180-5.

[133] C. Wu, J.W. McGinity, Non-traditional plasticization of polymeric films, International Journal of Pharmaceutics. 177 (1999) 15–27. https://doi.org/10.1016/S0378-5173(98)00312-3.
[134] M. Baiardo, G. Frisoni, M. Scandola, M. Rimelen, D. Lips, K. Ruffieux, E. Wintermantel, Thermal and mechanical properties of plasticized poly(L-lactic acid), Journal of Applied Polymer Science. 90 (2003) 1731–1738. https://doi.org/10.1002/app.12549.
[135] FTIR-spectroscopy in microbial and material analysis, International Biodeterioration & Biodegradation. 41 (1998) 1–11. https://doi.org/10.1016/S0964-8305(98)80002-4.
[136] A.C. Wilson, S.-F. Chou, R. Lozano, J.Y. Chen, P.F. Neuenschwander, Thermal and physico-mechanical characterizations of thromboresistant polyurethane films, Bioengineering (Basel). 6 (2019) E69. https://doi.org/10.3390/bioengineering6030069.
[137] Fingerprint Region, Chemistry LibreTexts. (2015). https://chem.libretexts.org/Ancillary_Materials/Reference/Organic_Chemistry_Glossary/Fingerprint_Region (accessed June 24, 2021).
[138] A. Enumo, I.P. Gross, R.H. Saatkamp, A.T.N. Pires, A.L. Parize, Evaluation of mechanical, thermal and morphological properties of PLA films plasticized with maleic acid and its propyl ester derivatives, Polymer Testing. 88 (2020) 106552. https://doi.org/10.1016/j.polymertesting.2020.106552.
[139] J.E. Oliveira, L.H.C. Mattoso, W.J. Orts, E.S. Medeiros, Structural and morphological characterization of micro and nanofibers produced by electrospinning and solution blow spinning: A comparative study, Advances in Materials Science and Engineering. 2013 (2013) e409572. https://doi.org/10.1155/2013/409572.
[140] J. Wu, Z. Zhang, J. Gu, W. Zhou, X. Liang, G. Zhou, C.C. Han, S. Xu, Y. Liu, Mechanism of a long-term controlled drug release system based on simple blended electrospun fibers, Journal of Controlled Release. 320 (2020) 337–346. https://doi.org/10.1016/j.jconrel.2020.01.020.